Available online at www.sciencedirect.com
ScienceDirect
Lithos 92 (2006) 336–356
LITHOS
www.elsevier.com/locate/lithos

Prograde garnet-bearing ultramafic rocks from the Tromsø Nappe, northern Scandinavian Caledonides☆

Erling J.K. Ravna *, Kåre Kullerud, Edel Ellingsen

Department of Geology, University of Tromsø, N-9037 Norway

Received 24 June 2005; accepted 30 March 2006
Available online 19 June 2006

Abstract

Garnet-bearing peridotitic rocks closely associated with eclogite within the Tromsø Nappe of the northern Scandinavian Caledonides show good evidence for prograde metamorphism. Early stages are recognized as inclusions of hornblende and chlorite in the cores of large garnet poikiloblasts. Closer to the garnet rim, clinopyroxene and Cr-poor spinel appear as additional inclusion phases. Four suites of spinel inclusions can be distinguished based on optical properties and chemical composition. The innermost suite (suite 1) has the lowest Cr# and highest Mg#. Further rimward, the spinel inclusions gradually change in composition, with increasing Cr# and decreasing Mg#. Spinel is rare in the matrix, but locally chromitic spinel occurs as larger grains. Garnet poikiloblasts are rimmed by a kelyphite zone consisting of Hbl+Cr-poor Spl or Opx±Cpx+Cr-poor Spl, and locally an inner zone of Na-rich Hbl+Chl. Matrix assemblage in the garnet-bearing peridotitic rocks is Hbl+Chl+Cpx+Ol±Cr-rich spinel, defining a strong foliation wrapping around garnets and associated kelyphites. Thin layers of garnet-orthopyroxenite and garnet–hornblende–zoisite–chlorite rocks are presumably coeval with the matrix foliation of the peridotitic rocks.

In dunitic to harzburgitic compositions large undulatory grains of Ol+Opx±Chl+Spl apparently define the maximum-*P* conditions. This assemblage is succeeded by a recrystallized assemblage of Ol±Tlc±Mgs, which in turn is overgrown by strain-free poikiloblasts of orthopyroxene, indicating a temperature increase. This is postdated by Tlc+Ath±Mgs, and finally serpentine.

P–T estimates for the inclusion suites of clinopyroxene and spinel in garnet clearly indicate garnet growth and spinel consumption in a regime of increasing *P*. The inner suite (suite 1) apparently was in equilibrium with garnet, clinopyroxene and olivine at 1.40 GPa, 675 °C, whereas included spinel with maximum Cr# (suite 4) indicate 2.40 GPa at 740 °C. Grt+Opx from garnet-orthopyroxenite give 1.5–1.9 GPa at 740–770 °C, and Grt+Hbl+Zo+Chl from a zoisite-rich rock give 1.75±0.25 GPa at 740±30 °C, interpreted to represent recrystallization during uplift. In dunitic to harzburgitic compositions, early Ol+Opx±Chl+Spl is succeeded by Ol±Tlc±Mgs, which in turn is overgrown by neoblasts of strain-free orthopyroxene, indicating temperature increase. This is postdated by Tlc+Ath±Mgs, and finally serpentine.

The ultramafic rocks in the Tromsø Nappe were locally strongly hydrated before subduction along with associated eclogites and metasedimentary rocks during the early (Ordovician) stages of the Caledonian orogeny.

Keywords: Garnet peridotite; HP/UHP metamorphism; Prograde; Caledonides

☆ Mineral abbreviations are after Kretz (1983).

* Corresponding author.
E-mail address: Erling.Ravna@ig.uit.no (E.J.K. Ravna).

0024-4937/$ - see front matter © 2006 Published by Elsevier B.V.
doi:10.1016/j.lithos.2006.03.058

1. Introduction

Garnet-bearing ultramafic rocks within HP and UHP terranes of continental collision zones have been described from various areas worldwide: The Scandinavian Caledonides (Medaris and Carswell, 1990 and references therein; Krogh and Carswell, 1995, and references therein; Carswell and Cuthbert, 2003, and references therein), the Bohemian Massif (Medaris et al., 1990; Medaris, 2000), the Dabie–Sulu terrane, China (Liou and Zhang, 1998; Zhang et al., 1994), the Alps (e.g. Ernst, 1978; Evans and Trommsdorff, 1978; Nimis and Morten, 2000; Obata and Morten, 1987; Paquin and Altherr, 2001) and Variscan Schwarzwald (Kalt and Altherr, 1996). These orogenic or "alpine type" garnet peridotites comprise a variety of rock types as lherzolite, harzburgite, wehrlite, dunite and pyroxenite. Experimental data clearly show that high pressures are necessary to stabilize garnet in peridotitic rocks. Bucher-Nurminen (1991) described alpine ultramafic rocks as "isolated single bodies, derived from the upper mantle emplaced within the crust by tectonic processes, and where composition, mineralogy and texture results from an orogenic event".

Most garnet peridotites are interpreted to represent slices of the overlying sub-continental mantle wedge which were incorporated in the subducting continental crust (Brueckner and Medaris, 2000; Medaris, 2000). Porphyroclasts of garnet and pyroxenes of these rocks commonly yield very high *P* and intermediate to high *T* estimates, whereas recrystallized neoblasts give lower *P* and *T*. Some garnet-bearing peridotitic rocks are, however, clearly formed from lower-*P* protoliths (e.g. spinel peridotite) within the continental crust, and were transformed into garnet peridotites during the subduction process.

Prograde HP/UHP meta-ultramafics have been documented in a few terranes. At Cima di Gagnone, garnet has overgrown pre-existing isoclinal folds involving all matrix materials, including Ca-amphibole and Ol+Ilm pseudomorphs after titanian clinohumite. Ca-amphibole included in garnet has distinctly higher K (0.7 wt.%) than those in the matrix (0.15 wt.%) (Evans and Trommsdorff, 1978). Evans and Trommsdorff (1978) interpreted the poikiloblastic peridotites from Cima di Gagnone as "subduction zone garnet peridotites" derived from a partially serpentinised, hydrous protolith. Prograde chlorite-amphibole peridotites are here commonly found to be isofacial with the garnet peridotites. The simultaneous occurrence of both rock types can be explained in terms of variable bulk composition and/or H_2O activity (Morten and Trommsdorff, 2003). Early spinel lherzolitic assemblages included in garnet are also described from garnet peridotites from Sulawesi, Indonesia (Kadarusman and Parkinson, 2000). In peridotites from the Nonsberg area, NE Italy, an early assemblage of Ol+Opx+Cpx+Spl± Amp is overprinted by higher-*P* garnet-bearing assemblages (Obata and Morten, 1987; Nimis and Morten, 2000). Garnet–spinel peridotites have also been described from the Variscan Schwartzwald (Kalt and Altherr, 1996).

This paper presents petrographical and petrological evidence for prograde HP metamorphism of low-*P* peridotitic rocks from the Tromsø Nappe, Northern Norway.

2. Geological setting

The Tromsø Nappe (earlier Tromsø Nappe Complex, e.g. Krogh et al., 1990), is the uppermost part of the Uppermost Allochthon of the Scandinavian Caledonides (Fig. 1). The Tromsø Nappe consists of a sequence of polymetamorphic high grade metasediments (garnet mica schist, marble, calc-silicates) with numerous bodies of mafic (eclogite and garnet amphibolite) and ultramafic rocks (Broks, 1985; Ellingsen, 1997; Krogh et al., 1990). Krogh et al. (1990) presented data on eclogites and associated gneisses from this area, indicating minimum *P* of 1.7–1.8 GPa at 700–750 °C, with a later overprint at c. 0.8–1.0 GPa/600–650 °C. More recent thermobarometers (Ravna and Terry, 2004) indicate, however, much a higher maximum *P* of 3.36 GPa (UHP) at c. 735 °C based on the assemblage Grt–Cpx–Phe (Ravna and Roux, in press). Partial melting of eclogite is fairly common (Krogh et al., 1990), and recent work by Stevenson (2005) confirms two episodes of partial melting. An early episode of melting producing peritectic garnet+melt occurred at 2.0–2.2 GPa, 762–844 °C, and a younger one producing peritectic hornblende+melt (garnet being a restite phase) at 1.0–1.3 GPa, 743–950 °C (Stevenson, 2005 and pers. com.).

Corfu et al. (2003) presented U–Pb zircon and titanite ages for the eclogitic rocks of the Tromsø Nappe. Apparently primary magmatic zircons from a trondhjemitic layer within the large Tromsdalstind eclogite (Krogh et al., 1990) gave an age of 493+5/−2 Ma, interpreted as the intrusion age of the protolith. Eclogitic zircons defined an age of 452.1±1.7 Ma, and similar ages of 451–450 Ma were also provided by high-Al titanites from an eclogite and a calc silicate rock. A low-Al titanite from a hornblende-bearing post eclogite leucosome gave 450.3±0.9 Ma, whereas a large rutile

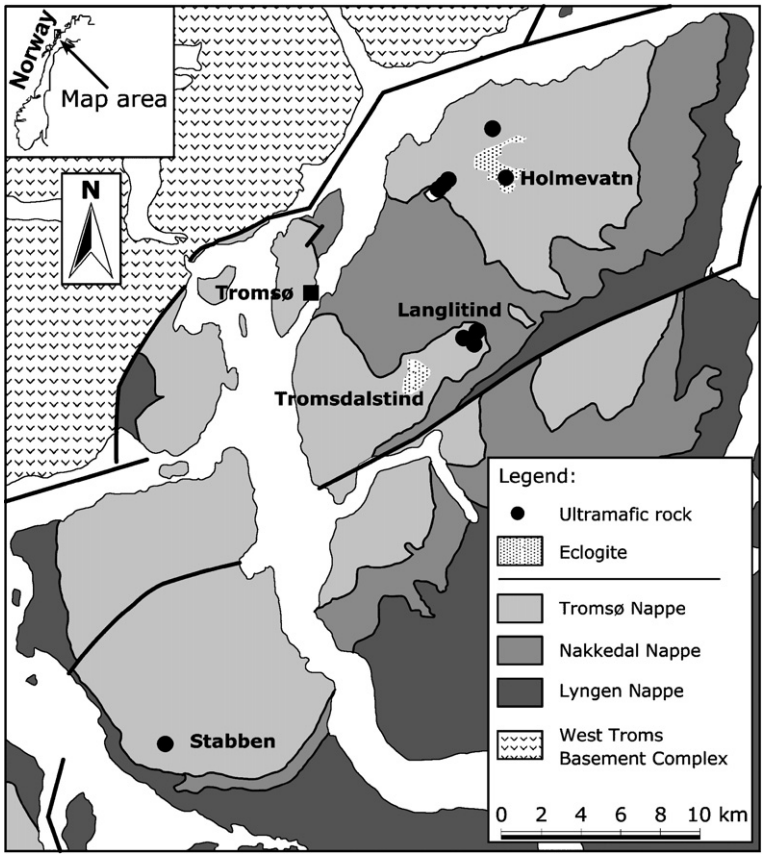

Fig. 1. Tectonostratigraphic map of the Tromsø area, showing the location of major bodies of eclogite and ultrabasic rocks in the Tromsø Nappe.

porphyroblast gave an age of 448.8±1.4 Ma. These results show that the HP/UHP event and subsequent uplift with partial melting of the eclogite happened within only a few million years (Corfu et al., 2003). A K–Ar age of late amphibole in a retrogressed eclogite gave 437±16 Ma (Krogh et al., 1990), and hornblende $^{40}Ar/^{39}Ar$ isotope correlation ages are reported within 419.4±2.1 and 481±1.8 Ma (Dallmeyer and Andresen, 1992).

The Tromsø Nappe is underlain by the Skattøra migmatite complex (Selbekk et al., 2000; Selbekk and Skjerlie, 2002) of the Nakkedal Nappe, and tectonically separated from it by a major thrust fault (Fig. 1). The Skattøra migmatite complex comprises an original Si-undersaturated (ne-normative) layered mafic complex with layers of anorthositic to ultramafic composition, with gabbroic compositions as the dominant type. The rocks have been subjected to a high degree of partial melting at high temperatures and H_2O, producing a network of anorthositic dikes dated to 456±4 Ma (Selbekk et al., 2000; Selbekk and Skjerlie, 2002).

Several small bodies of peridotitic rocks ranging in composition from olivine-poor garnet peridotite (Ca- and Al-richer; type 1) to dunitic (Ca- and Al-poor; type

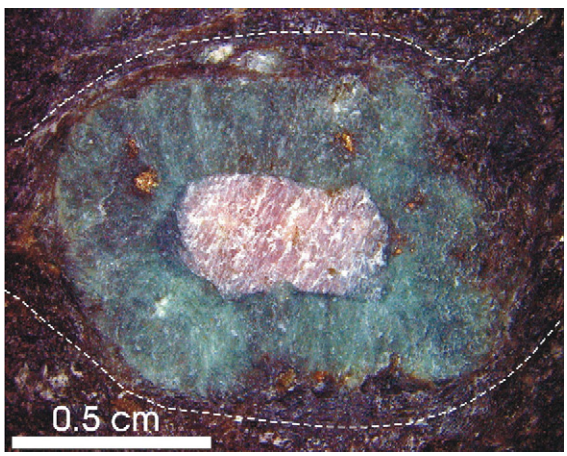

Fig. 2. Large garnet poikiloblast partly replaced by kelyphitic hornblende+spinel. Note that matrix foliation is wrapping around the garnet+kelyphite.

2) occur throughout the Tromsø Nappe. In this paper, three localities were studied in detail; two are of the type 2 and the third is of the type 1. Garnet has been found only in type 1 rocks.

2.1. Type 1 — Ca- and Al-rich peridotite

2.1.1. Holmevatn

A recently discovered type 1 peridotite in the Holmevatn area occurs in close proximity to a large eclogite body (Fig. 1). This ultramafic body is found as a few small (<5 m) outcrops in a bog close to the small lake Holmevatn). None of these bodies have been studied so far. Most of the outcrops are dunitic, but a tiny outcrop <1 m across consists of strongly foliated garnet peridotite, with garnet porphyroclasts of up to 3 cm across (Fig. 2), grading into less foliated, equigranular garnet peridotite, locally interlayered with thin bands of garnet-orthopyroxenite. The ultramafic rocks have a sharp transition to a pink, white and green rock consisting mainly of garnet, zoisite and hornblende.

2.2. Type 2 — Ca- and Al-poor peridotites

2.2.1. Langlitind

The ultramafic rock suite in Langlitind (Fig. 1) consists of one large lenticular (350×100 m) and several smaller irregular bodies. The foliation in the host garnet amphibolite wraps around massive ultramafic lenses. The main body is mainly composed of medium to coarse grained granoblastic dunite and porphyroblastic harzburgite. Major minerals are olivine and orthopyroxene, with minor hornblende in the harzburgite. Rosettes of anthophyllite needles, partially replaced by talc pseudomorphs occur on some fractures. Chlorite occurs sparsely distributed in the rock and also along fractures. The smaller bodies have cores of dunite/harzburgite, grading outwards to hydrated varieties composed of orthopyroxene, amphibole, talc, chlorite and minor carbonate. Cross-cutting granitic pegmatites typically show a reaction zone composed of biotite succeeded by Hbl+Chl toward the ultramafic host rock. Layers and lenses of chromitite (up to 30 cm thick) alternating with dunite/harzburgite

Table 1
Selected garnet analyses; structural formulae based on 12 oxygens

Locality	Holmevatn										
Rock type	Grt–Hbl perid	Grt–Hbl perid	Grt–Hbl perid	Grt–Hbl perid	Grt–Hbl perid	Grt–Hbl perid	Grt–Hbl perid		Grt-opxnite	Grt–Hbl–Zo	Grt–Hbl-Zo
Sample	UM-2A	UM-2B	UM-6	04028	04029	04029-1	04030		04031-1	04029-1A	04031
	At Cpx incl	Rim	At Cpx incl	Rim	Rim	Rim	Incl in Ol		Rim	Rim	Rim
							Min Mg#	Max Mg#			
SiO_2	41.84	41.71	41.80	41.69	41.72	42.14	40.61	41.76	41.95	42.00	41.74
Al_2O_3	22.71	22.98	23.26	23.01	23.46	23.51	22.92	23.48	23.46	23.53	23.34
TiO_2	0.00	0.00	0.00	0.00	0.00	0.00	0.00	0.00	0.00	0.00	0.00
Cr_2O_3	0.16	0.49	0.15	0.49	0.07	0.17	0.00	0.22	0.54	0.26	0.48
FeO	9.24	8.94	9.05	10.72	10.03	9.06	16.11	10.49	9.89	8.24	8.92
MnO	0.39	0.37	0.16	0.49	0.19	0.35	1.29	0.33	0.24	0.18	0.43
MgO	19.37	18.92	18.37	17.70	18.39	19.27	13.75	17.89	18.71	18.23	17.07
CaO	6.29	6.59	7.22	5.89	6.14	5.50	5.32	5.83	5.21	7.56	8.02
Total	100.00	100.00	100.01	100.00	100.00	100.00	100.00	100.00	100.00	100.00	100.00
12 Oxygens											
Si	2.99	2.98	2.99	3.00	2.99	3.00	3.00	3.00	3.00	3.00	3.00
Al	1.92	1.94	1.96	1.95	1.98	1.97	1.99	1.99	1.98	1.98	1.98
Ti	0.00	0.00	0.00	0.00	0.00	0.00	0.00	0.00	0.00	0.00	0.00
Cr	0.01	0.03	0.01	0.03	0.00	0.01	0.00	0.01	0.03	0.01	0.03
Fe^{2+}	0.55	0.54	0.54	0.65	0.60	0.54	0.99	0.63	0.59	0.49	0.54
Mn	0.02	0.02	0.01	0.03	0.01	0.02	0.08	0.02	0.01	0.01	0.03
Mg	2.07	2.02	1.96	1.90	1.96	2.04	1.51	1.91	1.99	1.94	1.83
Ca	0.48	0.51	0.55	0.45	0.47	0.42	0.42	0.45	0.40	0.58	0.62
Cations	8.04	8.03	8.02	8.01	8.02	8.01	8.00	8.00	8.00	8.01	8.00
Mg#	79	79	78	75	77	79	60	75	77	80	77

Totals of EDS analyses are normalized to 100%.

Table 2
Selected amphibole analyses; structural formulae based on 23 oxygens

Locality	Holmevatn													Langlitind				
Rock type	Grt–Hbl perid		Grt–Hbl perid					Grt–Hbl perid			Grt–Hbl perid	Grt–Hbl–Zo	Grt–Hbl–Zo	Dunite	Dunite	Amp–rich	Amp–rich	Harz
Sample	UM-2A		UM-2B					4028			4029	04029-1A	04031	45	52	43	43	54A
Mineral	Prg	Prg	Prg	Prg	Prg	Prg*	Tr	Prg	Prg	Tr	Prg	Prg	Cr–Prg	Tr	Tr	Ath	Tr	Tr
	Incl in Grt	Matrix	Incl in Grt	Matrix	Outer kelyph	Inner kelyph	Sec on Prg	Matrix	Kelyph w Spl	Recryst aggr	Matrix	Matrix	Matrix	Sec	Sec	sec	sec	sec
SiO_2	45.38	46.00	45.95	46.00	45.09	39.97	57.17	46.91	50.86	55.95	47.65	44.46	43.67	58.10	57.65	58.87	57.27	57.84
TiO_2	0.17	0.03	0.10	0.02	0.07	0.15	0.06	0.13	0.11	0.03	0.04	0.17	0.17	0.11	0.41	0.40	1.55	0.32
Al_2O_3	16.03	13.14	15.46	12.69	14.66	19.34	1.27	13.61	9.57	3.79	13.72	18.13	17.38	0.03	0.05	0.00	0.02	0.00
Cr_2O_3	0.22	0.84	0.37	0.92	0.15	0.23	0.14	0.82	0.18	0.08	0.24	0.69	2.20	0.18	0.07	0.23	0.01	0.09
FeO	2.88	4.56	2.99	5.62	4.89	7.66	2.51	4.18	3.19	2.37	3.24	2.78	2.25	1.41	2.26	8.04	2.61	1.13
MnO	0.00	0.00	0.00	0.00	0.00	0.00	0.00	0.09	0.12	0.00	0.04	0.07	0.13	0.07	0.05	0.31	0.02	0.04
MgO	18.34	18.32	18.66	18.36	17.72	16.04	23.19	18.10	20.20	21.95	18.79	17.30	17.48	23.42	23.45	29.23	23.05	23.58
CaO	12.47	12.35	12.25	11.71	12.09	10.27	12.98	12.39	12.45	12.98	11.90	11.22	11.57	12.98	12.19	0.46	12.40	13.11
Na_2O	2.40	2.44	2.17	2.49	3.15	3.97	0.60	1.60	1.17	0.77	2.23	3.00	3.01	0.11	0.38	0.09	0.38	0.13
K_2O	0.10	0.31	0.05	0.20	0.17	0.38	0.07	0.17	0.16	0.09	0.15	0.19	0.14	0.01	0.07	0.01	0.07	0.00
	98.00	98.00	98.00	98.00	98.00	98.00	98.01	98.00	98.00	98.01	98.00	98.00	98.00	96.42	96.58	97.64	97.38	96.24
23 oxygens																		
Si	6.32	6.48	6.39	6.50	6.36	5.68	7.82	6.56	7.03	7.65	6.62	6.19	6.11	8.01	7.96	7.97	7.86	7.98
Al	2.63	2.18	2.53	2.12	2.44	3.24	0.21	2.24	1.56	0.61	2.25	2.97	2.87	0.02	0.07	0.06	0.25	0.05
Ti	0.02	0.00	0.01	0.00	0.01	0.02	0.01	0.01	0.01	0.00	0.00	0.02	0.02	0.00	0.01	0.000	0.00	0.00
Cr	0.02	0.09	0.04	0.10	0.02	0.03	0.02	0.09	0.02	0.01	0.03	0.08	0.24	0.02	0.01	0.03	0.00	0.01
Fe^{3+}	0.00	0.00	0.00	0.00	0.00	0.50	0.00	0.00	0.00	0.00	0.00	0.00	0.00	0.00	0.00	0.00	0.00	0.0
Fe^{2+}	0.34	0.54	0.35	0.66	0.58	0.41	0.29	0.49	0.37	0.27	0.38	0.32	0.26	0.16	0.26	0.91	0.30	0.13
Mn	0.00	0.00	0.00	0.00	0.00	0.00	0.00	0.01	0.01	0.00	0.01	0.01	0.02	0.01	0.01	0.04	0.00	0.01
Mg	3.81	3.85	3.87	3.87	3.73	3.40	4.73	3.77	4.16	4.47	3.89	3.59	3.65	4.81	4.83	5.90	4.72	4.85
Ca	1.86	1.86	1.83	1.77	1.83	1.56	1.90	1.86	1.84	1.90	1.77	1.67	1.74	1.92	1.80	0.07	1.82	1.94
Na	0.65	0.67	0.59	0.68	0.86	1.09	0.16	0.43	0.31	0.21	0.60	0.81	0.82	0.03	0.10	0.02	0.10	0.04
K	0.02	0.06	0.01	0.04	0.03	0.07	0.01	0.03	0.03	0.02	0.03	0.03	0.03	0.00	0.01	0.00	0.01	0.0040
Cations	15.67	15.74	15.61	15.75	15.85	16.00	15.15	15.49	15.34	15.15	15.56	15.69	15.73	14.98	15.05	15.00	15.07	15.00
Mg#	92	88	92	85	87	89	94	89	92	94	91	92	93	97	95	87	94	97

Totals of EDS analyses are normalized to 98%.

Table 3
Selected chlorite analyses; structural formulae based on 28 oxygens

Locality	Holmevatn			Langlitind	Stabben			
Rock type	Grt–Hbl perid			Amph-rich	Dunite	Dunite	Harz	Dunite
Sample	UM-2A		UM-2B	43	45	52	54A	St8
	Aver incl	Av matr	Av inner kel	Matr	Matr	Matr	Matr	Matr
SiO_2	30.79	30.76	29.67	30.86	30.68	31.45	32.28	31.29
Al_2O_3	20.49	18.91	21.06	18.90	15.24	14.62	14.59	17.02
Cr_2O_3	0.25	0.80	0.12	0.92	1.96	2.02	2.10	2.29
FeO	3.25	3.97	7.46	3.43	4.34	4.24	1.40	2.28
MnO	0.00	0.00	0.00	0.00	0.02	0.00	0.03	0.04
MgO	31.22	31.57	27.70	32.23	32.26	32.72	33.43	31.98
	86.00	86.00	86.00	86.34	84.50	85.05	83.83	84.90
28 Oxygens								
Si	5.85	5.89	5.76	5.87	6.03	6.14	6.28	6.04
Al	4.59	4.27	4.82	4.24	3.53	3.36	3.35	3.87
Cr	0.04	0.12	0.02	0.14	0.30	0.31	0.32	0.35
Fe^{2+}	0.52	0.64	1.21	0.55	0.71	0.69	0.23	0.37
Mn	0.00	0.00	0.00	0.00	0.00	0.00	0.00	0.01
Mg	8.84	9.01	8.01	9.14	9.46	9.52	9.70	9.20
Cations	19.84	19.92	19.82	19.94	20.05	20.02	19.88	19.85
Mg#	94	93	87	94	93	93	98	96

Totals of EDS analyses are normalized to 86%.

Table 4
Selected spinel analyses; structural formulae based on 3 cations and 4 oxygens

Locality	Holmevatn									Langlitind			Stabben
Rock type	Grt–Hbl perid						Grt–Hbl perid	Grt–Hbl perid		Dunite	Dunite	Harz	Dunite
Sample	UM-2A						UM-6	04028		45	52	54A	St8
	Incl 1	Incl 1	Incl 2	Incl 3	Incl 4	Kel	In Ol	Chr core	Chr rim	Matrix	Matrix	Matrix	Matrix
	Min Cr	Aver	Aver	Aver	Max Cr	Aver							
TiO_2	0.00	0.00	0.00	0.00	0.00	0.00	0.00	0.00	0.00	0.12	0.12	0.17	0.03
Al_2O_3	65.71	64.36	61.93	58.00	37.53	63.37	36.71	24.12	37.03	0.66	0.44	1.97	12.02
Cr_2O_3	2.51	3.67	2.95	5.36	24.68	0.62	26.58	40.36	27.40	26.83	17.04	49.36	52.97
FeO	7.45	8.97	16.45	21.64	30.64	17.19	24.13	25.78	21.69	58.65	76.12	40.50	27.74
MnO	0.00	0.00	0.00	0.00	0.00	0.00	0.00	0.21	0.25	0.41	0.35	0.35	0.28
MgO	24.33	22.99	18.67	15.00	7.15	18.82	12.59	9.53	13.64	2.85	1.86	4.76	5.94
	100.00	100.00	100.00	100.00	100.00	100.00	100.00	100.00	100.01	89.52	95.93	97.11	98.98
Normalized cations													
Al	1.91	1.89	1.87	1.81	1.33	1.91	1.26	0.89	1.26	0.03	0.02	0.08	0.48
Ti	0.00	0.00	0.00	0.00	0.00	0.00	0.00	0.00	0.00	0.00	0.00	0.00	0.00
Cr	0.05	0.07	0.06	0.11	0.59	0.01	0.61	0.99	0.62	0.84	0.50	1.41	1.42
Fe^{3+}	0.05	0.04	0.07	0.07	0.09	0.08	0.13	0.12	0.12	1.12	1.47	0.49	0.10
Fe^{2+}	0.11	0.15	0.29	0.41	0.68	0.28	0.45	0.56	0.42	0.82	0.89	0.74	0.69
Mn	0.00	0.00	0.00	0.00	0.00	0.00	0.00	0.01	0.01	0.01	0.01	0.01	0.01
Mg	0.89	0.85	0.71	0.59	0.32	0.72	0.55	0.44	0.59	0.17	0.10	0.26	0.30
Cations	3.00	3.00	3.00	3.00	3.00	3.00	3.00	3.00	3.00	3.00	3.00	3.00	3.00
Mg#	89	85	71	59	32	72	55	44	59	13	7	24	30
X(Cr)	0.02	0.04	0.03	0.06	0.29	0.01	0.31	0.50	0.31	0.42	0.25	0.71	0.71

Totals of EDS analyses are normalized to 100%.

Table 5
Selected pyroxene analyses; structural formulae based on 6 oxygens

Locality	Holmevatn											Langlitind		Stabben					
Rock type	Grt–Hbl perid	Grt–Hbl perid	Grt–Hbl perid	Grt–Hbl perid			Grt–Hbl perid	Grt–Hbl rock	Grt-opxnite	Grt–Hbl perid	Grt-opxnite	Dunite	Dunite	Harz	Dunite	Amph–rich	Dunite		
Sample	UM-2A	UM-6	UM-2B	04028			04029	04029A	04029-1	04030	04031-1	45	45	54A	52	43	Si8		
Mineral	Cpx	Cpx	Cpx	Cpx	Cpx	Opx	Cpx	Opx	Opx	Opx	Opx	Opx	Opx	Opx	Opx	Opx	Host Opx	Cpx lam	re–int
	Incl	Incl	Matrix	Matrix	Kel	Kel	In grt	Matrix	Matrix	Kel	Matrix	Matrix	Matrix	matrix	matrix	matrix			
SiO_2	54.41	54.16	55.02	54.45	54.72	55.76	55.00	56.98	56.84	55.76	56.81	57.37	58.59	58.51	58.08	57.11	58.25	54.27	57.80
Al_2O_3	1.63	1.86	0.55	1.59	1.31	2.45	1.51	1.96	2.01	2.48	1.99	0.12	0.04	0.09	0.11	0.69	0.26	1.06	0.35
TiO_2	0.00	0.00	0.00	0.00	0.00	0.00	0.00	0.00	0.00	0.00	0.00	0.02	0.02	0.00	0.00	0.03	0.00	0.00	0.00
Cr_2O_3	0.47	0.24	0.09	0.21	0.07	0.09	0.18	0.26	0.00	0.12	0.20	0.06	0.04	0.04	0.00	0.12	0.06	0.66	0.13
FeO	2.05	1.91	2.12	2.17	2.06	9.13	1.66	6.52	5.87	9.14	6.51	5.18	5.43	3.45	5.79	7.95	5.60	1.48	5.14
MnO	0.00	0.00	0.00	0.07	0.00	0.25	0.07	0.07	0.00	0.28	0.20	0.17	0.21	0.08	0.14	0.10	0.15	0.06	0.14
MgO	17.00	17.39	17.44	17.48	17.53	32.11	17.49	34.01	35.03	32.09	34.13	35.38	35.98	36.45	35.28	33.36	35.57	17.21	33.51
CaO	24.09	24.05	24.55	23.55	23.89	0.21	23.60	0.21	0.25	0.15	0.16	0.07	0.11	0.06	0.08	0.11	0.10	25.16	2.92
Na_2O	0.35	0.38	0.24	0.48	0.43	0.00	0.49	0.00	0.00	0.00	0.00	0.00	0.00	0.00	0.00	0.00	0.00	0.10	0.01
Total	100.00	100.00	100.00	100.00	100.00	100.00	100.0	100.01	100.00	100.01	100.00	98.37	100.42	98.68	99.48	99.47	100.00	100.00	100.00
Structural formulae based on 6 oxygens																			
Si	1.97	1.96	2.00	1.97	1.98	1.95	1.99	1.96	1.95	1.95	1.96	2.00	2.00	2.01	2.00	1.99	1.98	1.97	1.98
Al	0.07	0.08	0.02	0.07	0.06	0.10	0.06	0.08	0.08	0.10	0.08	0.00	0.00	0.00	0.00	0.00	0.03	0.05	0.04
Ti	0.00	0.00	0.00	0.00	0.00	0.00	0.00	0.00	0.00	0.00	0.00	0.00	0.00	0.00	0.00	0.00	0.000	0.00	0.00
Cr	0.01	0.01	0.00	0.01	0.00	0.00	0.01	0.01	0.00	0.00	0.01	0.00	0.00	0.00	0.00	0.00	0.00	0.02	0.01
Fe	0.06	0.06	0.06	0.07	0.06	0.27	0.05	0.19	0.17	0.27	0.19	0.15	0.16	0.10	0.17	0.23	0.17	0.05	0.16
Mn	0.00	0.00	0.00	0.00	0.00	0.01	0.00	0.00	0.00	0.01	0.01	0.01	0.01	0.00	0.00	0.00	0.01	0.00	0.01
Mg	0.92	0.94	0.94	0.94	0.95	1.67	0.94	1.75	1.79	1.67	1.75	1.84	1.84	1.87	1.81	1.73	1.80	0.93	1.72
Ca	0.94	0.93	0.95	0.91	0.93	0.01	0.91	0.01	0.01	0.01	0.01	0.00	0.00	0.00	0.00	0.00	0.01	0.98	0.10
Na	0.02	0.03	0.02	0.03	0.03	0.00	0.03	0.00	0.00	0.00	0.00	0.00	0.00	0.00	0.00	0.00	0.00	0.01	0.00
Sum	4.00	4.01	4.00	4.01	4.01	4.00	4.00	3.99	4.01	4.00	4.00	4.00	4.00	3.99	3.99	3.99	4.00	4.00	4.00
Mg#	94	94	94	93	94	86	95	90	91	86	90	92	92	95	92	88	91	95	92

Totals of EDS analyses are normalized to 100%.

Table 6
Selected olivine analyses; structural formulae based on 4 oxygens

Locality	Holmevatn										Langlitind		Stabben
Rock type	Grt–Hbl perid		Grt–Hbl perid		Grt–Hbl perid		Grt–Hbl perid	Grt–Hbl perid	Grt–Hbl perid		Dunite	Dunite	Dunite
Sample	UM-2A		UM-2B		UM-6		04028	04029	04030		45*	52*	St8
	Max Fo	Min Fo	Max Fo	Min Fo	Max Fo	Min Fo	Matr	Matr	Ol at Grt incl	Ol in matrix			
SiO_2	40.38	39.56	40.18	39.64	39.70	40.50	40.51	39.92	39.27	40.34	40.92	40.79	40.58
FeO	12.85	15.35	12.11	15.95	12.38	13.20	11.73	12.79	17.27	12.84	7.37	8.57	8.09
MnO	0.37	0.21	0.34	0.19	0.06	0.06	0.00	0.00	0.11	0.00	0.11	0.10	0.10
MgO	46.25	44.20	46.80	43.84	47.76	46.13	47.76	47.29	43.11	46.82	50.58	49.89	50.16
NiO	0.00	0.00	0.00	0.00	0.00	0.00	0.00	0.00	0.00	0.00	0.39	0.48	0.46
CaO	0.16	0.68	0.57	0.38	0.10	0.11	0.00	0.00	0.24	0.00	0.02	0.00	0.00
Total	100.01	100.00	100.00	100.00	100.00	100.00	100.00	100.00	100.00	100.00	99.39	99.83	99.39
4 oxygens													
Si	1.00	1.00	1.00	1.00	0.99	1.01	1.00	0.99	1.00	1.00	1.00	1.00	1.00
Fe	0.27	0.32	0.25	0.34	0.26	0.27	0.24	0.27	0.37	0.27	0.15	0.18	0.17
Mn	0.01	0.00	0.01	0.00	0.00	0.00	0.00	0.00	0.00	0.00	0.00	0.00	0.00
Mg	1.71	1.66	1.73	1.65	1.77	1.71	1.76	1.75	1.63	1.73	1.84	1.82	1.83
Ni	0.00	0.00	0.00	0.00	0.00	0.00	0.00	0.00	0.00	0.00	0.01	0.01	0.01
Ca	0.00	0.01	0.01	0.01	0.00	0.00	0.00	0.00	0.01	0.00	0.00	0.00	0.00
Sum	3.00	3.00	3.00	3.00	3.01	2.99	3.00	3.01	3.00	3.00	3.00	3.00	3.00
Mg#	87	84	87	83	87	86	88	87	82	87	92	91	92

Totals of EDS analyses are normalized to 100%.

are locally found. The oldest generation of fractures are filled with magnesite+talc, or anthophyllite, while younger fractures contain chlorite or talc, with some serpentine.

2.2.2. Stabben

The Stabben ultramafic body is located on the SW part of the Malangen peninsula (Fig. 1). Four ultramafic bodies occur along strike within a series of garnet mica schist, marble, quartzfeldspathic gneiss and amphibolite, close to the hinge of a large syncline. The main body appears as a nearly cylindrical body with a diameter of 150 m, towering about 70 m above the surroundings. The contact with the surrounding rocks is not exposed. To the west and northwest, three other bodies occur, but they are more altered and covered by moraine. In this work, most observations are taken from the Stabben locality. The main rock is a medium to coarse grained massive dunite, grading into harzburgite. Olivine makes up 70 to >90% of the rock. Orthopyroxene is coarser than olivine, and shows wavy shiny cleavage planes. On weathered surfaces the rock has a "warty" appearance due to the orthopyroxene being more resistant than olivine to weathering. Early fractures, filled with talc and magnesite, are up to 1–2 cm wide, whereas a younger generation has bright green amphibole±purple chlorite (kämmererite). The last generation of fractures is filled with asbestos serpentine.

Other smaller bodies are composed of harzburgite, occurring as lenses in a serpentinitic and talc-rich matrix. Fractures are filled with chlorite, serpentine, talc and carbonate.

3. Analytical procedures

Selected mineral compositions are given in Tables 1–7. The samples from Holmevatn were analyzed with a JEOL 840 SEM with an EDAX analyzer, using the EDAX SEM-Quant standardless method with optimized SEC factors based on analyses of a set of various mineral standards. Operating conditions were 20 kV accelerating voltage and a beam current of 3 nA. Anhydrous minerals (garnet, spinel, pyroxene and olivine) are normalized to a total of 100 wt.%, amphiboles to a total of 98 wt.%, and chlorite to 86 wt.%. Minerals from the Langlitind and Stabben bodies were analyzed on a CAMECA CAMEBAX microprobe at the Mineralogical–Geological Museum, University of Oslo, using an accelerating voltage of 15 kV and a beam current of 20.5 nA. These two

methods produce analyses that are within uncertainty limits for major and minor elements on a structural formula basis.

4. Petrography

4.1. Holmevatn

Garnet occurs in different textural settings in the Holmevatn peridotites. Those in strongly foliated Ca–Al-rich layers occur as large (up to 40 mm across) poikiloclasts in a matrix of Hbl+Chl+Cpx±Ol±Spl (Fig. 2). Common inclusions of chlorite and hornblende are found in the central part of the largest garnets. Within the intermediate zones of these garnets, clinopyroxene and Cr-poor spinel appear along with hornblende and chlorite (Fig. 3a). In the less foliated and olivine rich part of this body, garnet occurs as finer grained aggregates together with diopside between large olivine porphyroclasts. Olivine and garnet is always separated by a rim of kelyphite consisting either of Hbl+Spl or Opx+Spl±Cpx, except for one sample where smaller garnets are enclosed in olivine. Toward the contact with the garnet–hornblende–zoisite rock, thin bands of garnet-orthopyroxenite occur (Fig. 4b).

In all rock types, garnet is Mg-rich and Ca-poor. Zoning is not regular, and composition may vary locally along fractures. Mg-number (Mg#=100*Mg/(Mg+Fe)) ranges from 75 to 80 (Table 1), but may be more extreme within single grains, as shown by a small garnet enclosed in olivine in sample 04030 (Mg#=60–75). X_{ca} is lowest in garnet from garnet-orthopyroxenite (0.40–0.42 apfu), and highest in the garnet–hornblende–zoisite rocks (0.58–0.62 apfu). In the garnet–hornblende–zoisite rock a rimward increase of Ca and a consequent Mg-decrease is found.

Kelyphites are always present around garnet poikiloblasts (Fig. 2). Many garnet grains are rimmed by fine kelyphites of Hbl+Spl (Figs. 2, 3a and 5c). Locally, an inner separate kelyphite zone containing Na-rich Hbl+Chl is present (Fig. 5d). In more Ca- and Al-poor domains kelyphites of Opx±Cpx+Spl is developed, with an Al-poor zone consisting of Opx+Cpx located next to olivine (Fig. 5b). The spinel in the kelyphite zones is low in Cr (Fig. 3b), and has intermediate $X_{Fe^{2+}}$ (0.23–0.34).

Hornblende (pargasite) is a major mineral in the Ca- and Al-rich garnet peridotites. It occurs as inclusions in garnet (Fig. 3a) and as the principal matrix mineral defining, together with chlorite and diopside, the main foliation of these rocks (Fig. 4a). Inclusions in garnet appear to be richer in the tschermakite molecule than those in the matrix, and they also have a distinctly higher Mg# (Fig 6a–c; Table 2). The matrix amphibole is fairly similar to that in the outer kelyphite zone (Fig. 6a–c). Trace tremolite is present as secondary growths on matrix pargasite. Hornblende in the garnet–hornblende–zoisite rock is relatively rich in Cr.

Chlorite is present both as inclusions in garnet and as a major phase making up the main foliation of the matrix in the Ca–Al–rich compositions (Fig. 4a). The Mg# and Al^{tot} of the inclusions (94 and 4.59 apfu on average) is higher than in the matrix chlorite (93 and 4.27 apfu) (Table 3). Chlorite in the inner kelyphite zone of some garnets has lower Mg# (87), but high Al^{tot} (4.82 apfu). Chlorite veins cross-cutting or replacing garnet is relatively Fe-rich.

Spinel occurs mainly as inclusions in garnet from Al-rich compositions, and as composite inclusions of Hbl+Chl+Spl (Fig. 3a). Discrete spinel grains within the Hbl+Spl kelyphite zone are former inclusions in garnet rather that a secondary product. The color of spinel inclusions changes outward in the garnet and further into the kelyphite zone. Four suites of spinel

Table 7
Analyses of Mg-staurolite and zoisite; structural formulae based on 48 and 12.5 oxygens, respectively

Locality	Holmevatn			
Rock type	Grt–Hbl–Zo rock			
Sample	04029-1	04031	04029-1	04031
Mineral	Mg–St in grt	Cr–Mg–St	Zo	Zo
SiO_2	27.58	28.52	40.32	40.44
Al_2O_3	59.38	53.61	33.79	33.53
Cr_2O_3	0.18	5.63	0.18	0.47
Fe_2O_3	0.00	0.00	0.86	0.48
FeO	4.27	3.59	0.00	0.00
MnO	0.00	0.00	0.00	0.00
MgO	8.10	8.35	0.00	0.00
ZnO	0.50	0.31	0.00	0.00
CaO	0.00	0.00	24.84	25.07
	100.00	100.00	99.99	100.00
	48 oxygens		12.5 oxygens	
Si	7.51	7.86	3.00	3.01
Al	19.05	17.42	2.96	2.94
Ti	0.00	0.00	0.00	0.00
Cr	0.04	1.23	0.01	0.03
Fe^{3+}	0.00	0.00	0.05	0.03
Fe^{2+}	0.97	0.83	0.00	0.00
Zn	0.10	0.06	0.00	0.00
Mn	0.00	0.00	0.00	0.00
Mg	3.28	3.43	0.00	0.00
Ca	0.00	0.00	1.98	2.00
Cations	30.95	30.82	7.99	8.00

Totals of EDS analyses are normalized to 100%.

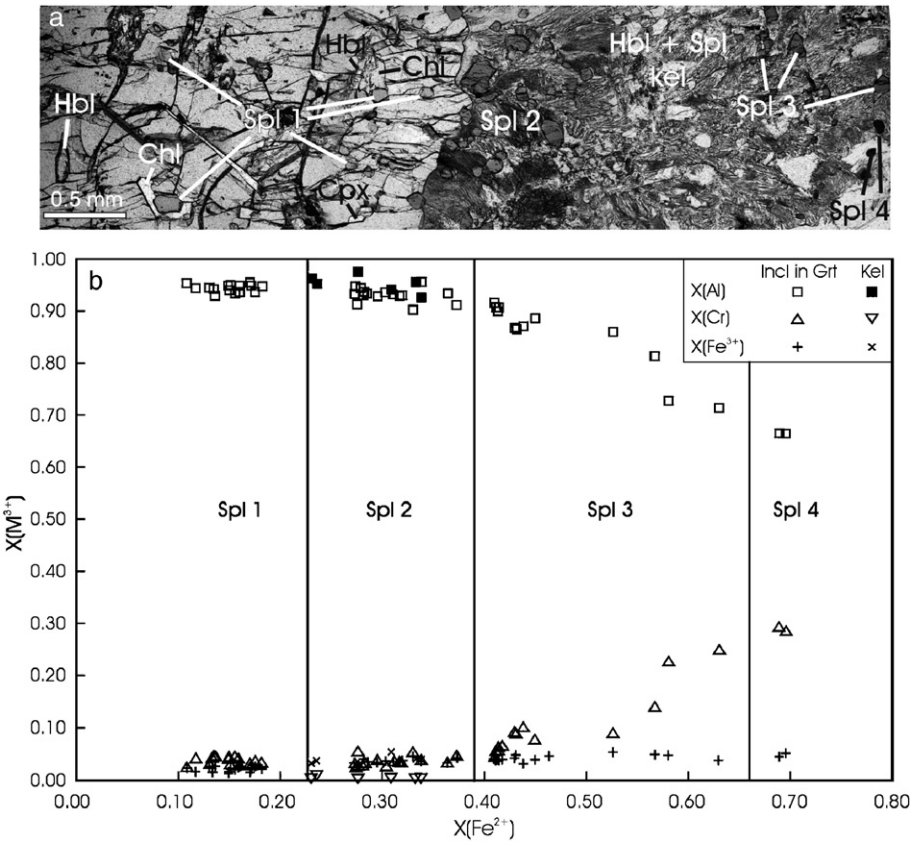

Fig. 3. (a) Successive inclusions of spinel in large garnet poikiloblast, extending into the hornblende + spinel kelyphite zone. Inclusions of hornblende, clinopyroxene and chlorite are also shown; (b) chemical variation of spinel inclusions related to their position within the garnet. Sample UM-2A.

inclusions can be distinguished based on optical characteristics. The innermost inclusions (suite 1) have a pale pink color, whereas suite 2 spinel is pale to dark green, while suite 3 is olive green, and spinel in the outermost part of the kelyphite zone (suite 4) is brownish green (Fig. 3a); such color change is consistent with compositional variation with increasing $X_{Fe^{2+}}$ (0.11–0.69) and Cr-content $\left(Cr = \frac{100*Cr}{Cr+Al+Fe^{3+}}\right) = 4 - 20$ (Fig. 3b; Table 4). The larger spinel grains within the kelyphite zone have a composition distinct from the kelyphitic spinel (Fig. 5b–d; Fig. 3b).

In the olivine-rich assemblage, large porphyroblasts of chromite are present locally.

Clinopyroxene occurs (1) as inclusions in garnet (Fig. 3a), (2) as a matrix phase together with Hbl + Chl ± Ol in the foliated matrix (Fig. 4a) of the most Ca- and Al-rich peridotites, (3) together with garnet aggregates between large olivine porphyroclasts in the olivine-rich layers, and (4) as a part of kelyphites after garnet, together with spinel and orthopyroxene (Fig. 5b). Clinopyroxene inclusions in garnet have the highest content of Al and Mg# (Table 5). The content of Na and Cr is low.

Orthopyroxene has only been found in the garnet–orthopyroxene rich laminae and in the olivine-rich layers, both as separate grains (En_{90}) (Fig. 4b) and as part of Opx–Spl–Cpx kelyphites (En_{86}) (Fig. 5b). In the garnet-orthopyroxenite, orthopyroxene occurs either as equidimensional subhedral grains or as anhedral poikiloblasts, including small grains of garnet. The Al-content of orthopyroxene varies, and is lowest in the core of the equidimensional subhedral grains (ca. 2.00 wt.% Al_2O_3). Orthopyroxene in kelyphite has an Al_2O_3 content of 2.0–2.45 wt.%.

Olivine in the Holmevatn dunitic body occurs as equigranular mosaic textured groundmass together with orthopyroxene. In the Ca–Al poor peridotitic varieties, olivine occurs both as larger porphyroblasts and as smaller mosaic textured grains surrounding the strained porphyroclasts. The composition varies (Table 6) within the range $Fo_{88–82}$. Even in a single domain of a thin section, olivine shows a distinct chemical variation of Fo_{87}–Fo_{82}.

Zoisite is a major mineral in the garnet–hornblende–zoisite rock and is low in Fe^{3+}(Table 7).

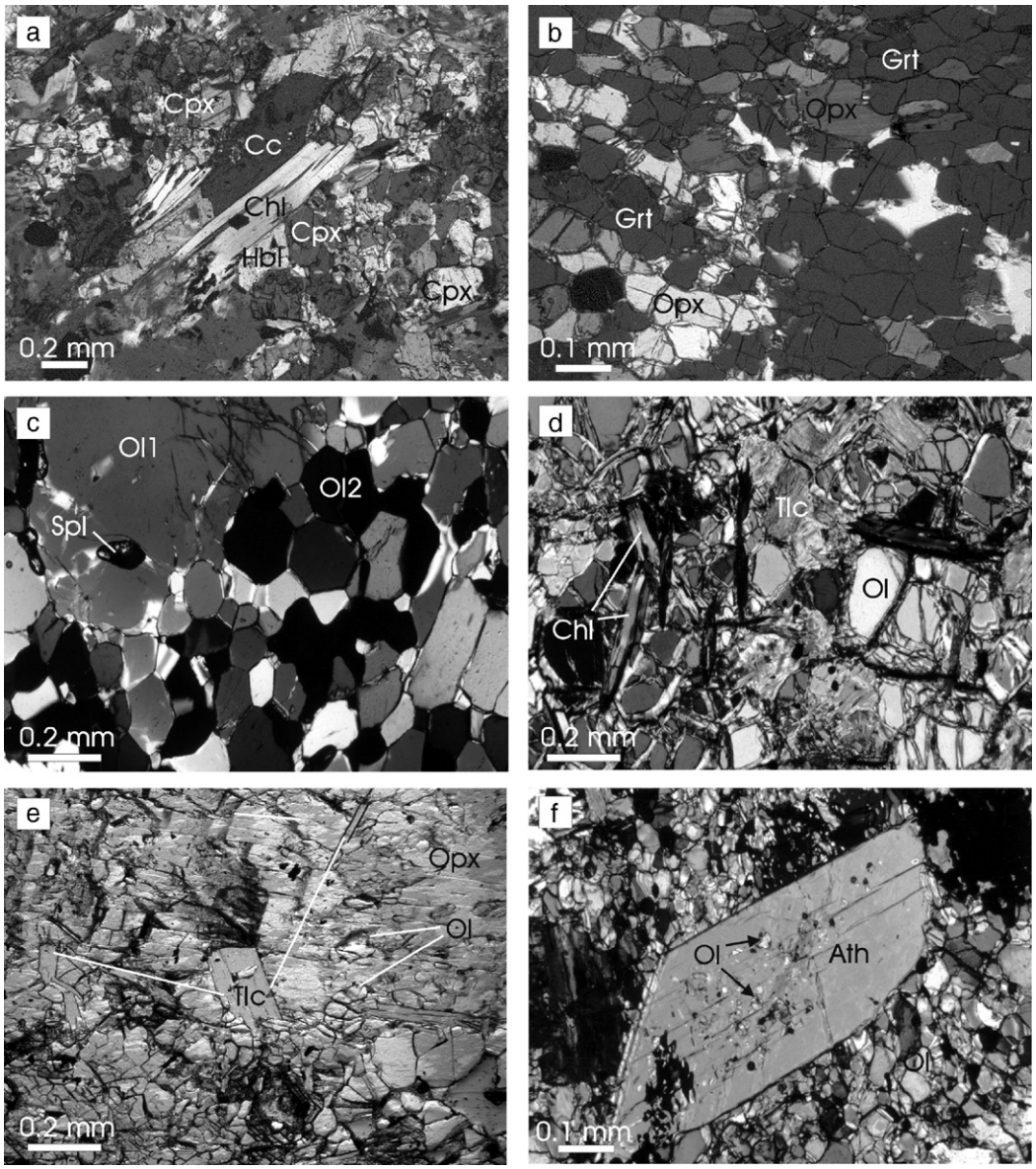

Fig. 4. Textural relationships in various rock types. (a) Matrix assemblage of clinopyroxene+hornblende+chlorite+calcite in Ca–Al rich sample UM-2B, Holmevatn; (b) recrystallized garnet–orthopyroxene in garnet-orthopyroxenite sample 04029-1; Holmevatn; (c) large early porphyroclast with inclusion of Cr-rich spinel, and recrystallized neoblasts of olivine in dunite, Stabben; (d) recrystallized matrix of olivine+talc+chlorite from Langlitind dunite. Olivine is partly serpentinised; (e) large poikilitic orthopyroxene with inclusions of the matrix phases olivine+talc, Langlitind; (f) large poikiloblast of anthophyllite with inclusions of the matrix phase olivine, Langlitind.

Other rare mineral inclusions include albite in garnet, close to the inner Na-rich kelyphite zone (Fig. 5d), and Mg- and Mg–Cr-staurolite in garnet and pargasite in the garnet–hornblende–zoisite rock (Table 7). Mg- and Cr-staurolite has been reported in various rock types from Fiordland, New Zealand (Ward, 1984), Vohibory, Madagascar (Nicollet, 1986), Donghai, China (Enami and Zhang, 1988) and Cabo Ortegal, NW Spain (Ibarguchi et al., 1991).

4.2. Stabben and Langlitind

Olivine occurs as anhedral grains up to 6 cm across in dunite. Deformation results in straining of large grains, with recrystallization to smaller unstrained grains, locally containing inclusions of spinel (Fig. 4c). The composition of olivine is in the range Fo_{90}–Fo_{92} (Table 6). There is no difference in composition of large strained grains and small recrystallized grains. Olivine

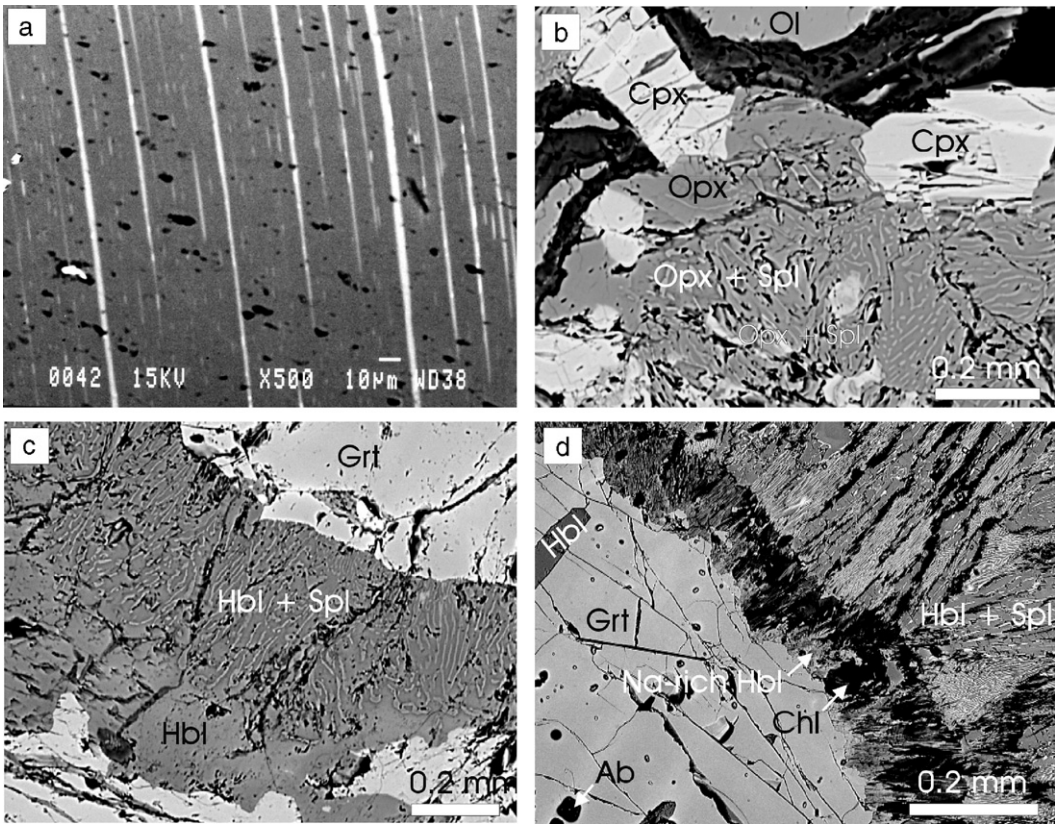

Fig. 5. BSE images of UM-rocks. (a) Exsolved lamellae of clinopyroxene in orthopyroxene porphyroclasts, Stabben dunite; (b) orthopyroxene–spinel kelyphite between garnet and olivine, with clinopyroxene+orthopyroxene next to olivine, sample 04028, Holmevatn; (c) hornblende+spinel kelyphite between garnet poikiloblast and matrix rich in clinopyroxene+hornblende, sample UM-2A, Holmevatn; (d) two kelyphitic zones developed around garnet. Inclusions of hornblende and pure albite in garnet. Sample UM-2B, Holmevatn.

in serpentinites appears to be more Fe-rich than those from dunite.

Orthopyroxene ($En_{87–96}$; Table 5) appears as dark green to golden brown short prismatic crystals in harzburgitic to dunitic rocks, and comprises up to 20% of the rock. In some Stabben samples lamellae of clinopyroxene oriented parallel to (100) in orthopyroxene is observed (Fig. 5a), preferentially within the core of larger grains. These grains are strained and commonly elongated, showing recrystallization along the margins. Unstrained orthopyroxene poikiloblasts with numerous small inclusions of olivine, talc and trace magnesite are present (Fig. 4e). Orthopyroxene breakdown to amphibole and chlorite along cleavage planes is a common feature, and anthophyllite may partly to totally replace orthopyroxene.

Spinel (sensu lato) is present in all rock varieties (Table 4). Spinel (sensu stricto) occurs as amoeboid grains in the dunites from Stabben. *Chromite* is more common than spinel (sensu stricto), and occurs in different settings, as small grains among olivine, as poikiloblasts with fine-grained inclusions of mostly chlorite, and as inclusions in recrystallized olivine. Magnetite occurs as euhedral grains in the most extensively altered rocks.

Anthophyllite (Mg# 86–88) occurs mainly in rosette-like aggregates in fractures as long prismatic colorless to faintly yellowish brown crystals, commonly <1 cm long, but occasionally up to 10 cm. In the matrix it is a minor phase, but it constitutes a major mineral in more amphibole-rich zones. It is a common replacement product of orthopyroxene, initially growing along cleavage planes and eventually replacing the whole grain. Locally, large poikiloblasts of anthophyllite with inclusions of olivine occur in harzburgitic layers (Fig. 4f). Anthophyllite, in turn, is replaced by talc or serpentine and contains low Al and Na.

Tremolite (1–5 mm, locally up to 5 cm) and pale brown *tremolitic hornblende* (<1 mm) both occur as acicular grains on fracture surfaces or as a reaction product after orthopyroxene. Tremolitic hornblende is less common than tremolite. Both are partially to totally

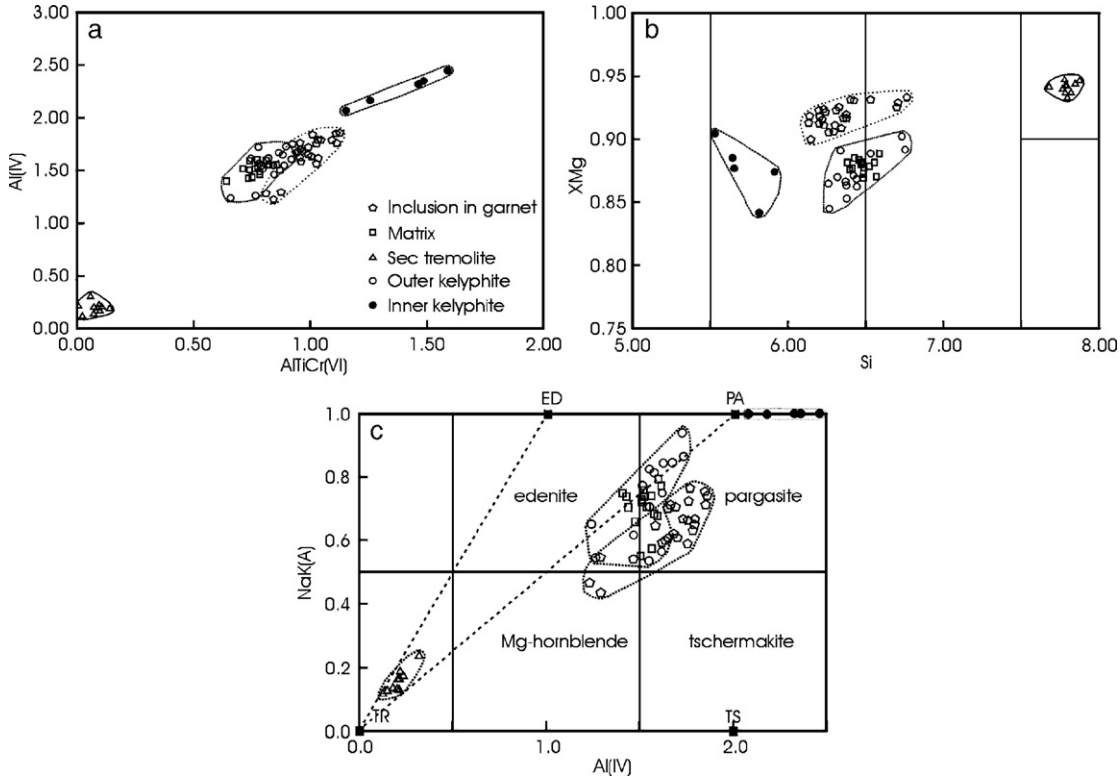

Fig. 6. Chemical variation of hornblende in terms of textural appearance, sample UM-2A. (a) X_{Mg} = Mg/(Mg + Fe) vs. Si; (b) Al(IV) vs. AlCrTi(VI); (c) Al(IV) vs. NaK(A).

replaced by talc and serpentine. High Cr-content is found in deep green colored crystals in fractures of the Stabben body. There appears to be a continuous compositional variation from tremolite to tremolitic hornblende.

Chlorite, green to purple, occurs as flaky crystals distributed throughout the matrix, and as larger crystals along fractures and pegmatitic veins. Chlorite is Mg-rich; the Fe-content increases with the degree of alteration of the rock. Chlorite is commonly associated with spinel, and Cr-rich varieties (kämmererite) are typically found around chromite. In one sample, an aggregate of chlorite in dunite apparently mimics the crystal shape of a former garnet. Chlorite is partially replaced by talc and serpentine. The Cr-content increases with increasing degree of alteration.

Talc occurs locally in apparent equilibrium with olivine and chlorite (Fig. 4d), and as separate inclusions together with olivine in large orthopyroxene poikiloblasts (Fig. 4e). Most talc grains are replacing other minerals and also occur as flaky aggregates together with serpentine, chlorite or amphibole on fracture surfaces. Talc is also seen as pseudomorphs after anthophyllite.

Serpentine is fine-grained and fibrous, yellowish green or grayish. It occurs in fractures, both along network thin fractures in olivine grains and in wider fractures of the rocks. It forms pseudomorphs after other minerals and is most common in the strongly hydrated rocks. Antigorite appears as platy grains overgrowing older minerals and is the most common variety in serpentinites. The fibrous varieties lizardite and chrysotile occur as pseudomorphs after other minerals and as a network of veins cross-cutting earlier minerals.

Magnesite (Mg# 93–96) occurs as a reaction product after other minerals, commonly in the outer part of the different bodies, along fractures and veins, and as poikiloblastic grains with inclusions of olivine. Calcite is locally found in serpentinised domains.

5. Textural evolution

5.1. Textural development in the Ca–Al-rich garnet-bearing ultramafics

The earliest pre-high-*P* stage is found in Al-rich compositions from Holmevatn as inclusions of chlorite, hornblende, clinopyroxene and Cr-poor spinel in large

garnet poikiloblasts. Polyphase inclusions of Hbl+Chl+Spl are common (Fig. 3a). The successive compositional change of spinel from Cr#=2–30 and $X_{Fe^{2+}} = 0.11 - 0.70$ outwards in the garnet/kelyphite zone clearly indicates increasing *P* during garnet growth at the expense of the included minerals. Based on the observed textural relations we suggest the following succession of mineral assemblages:

- Ia. Hbl+Chl+Cpx+low-Cr Spl+Ol
- IIa. Hbl+Chl+Cpx+higher-Cr Spl+Grt+Ol
- IIIa. Hbl+Chl+Cpx+Grt+Ol (max-*P*?)
- IVa. Hbl+Chl+Cpx+Grt+Ol (post max-*P* recrystallization)
- IVa′. Grt+Opx±Hbl in garnet-orthopyroxenite
- Va1. Opx±Cpx+low-Cr Spl (kelyphite 1a; decompression)
- Va2. Hbl+low-Cr Spl (kelyphite 1b; decompression)
- VIa. Na-rich Hbl+Chl (kelyphite 2; decompression)
- VIIa. Tr+Chl+Srp.

Because the foliated matrix assemblage wraps around both the large garnet poikiloblasts and their totally undeformed kelyphitic daughter products, we suggest that this foliation was formed before the kelyphites, but after the final stages of garnet growth, and may thus represent a recrystallized max-*P* assemblage. The sub-assemblages of Grt+Opx in the garnet-orthopyroxenite layers and the Grt+Hbl+Zo±Chl in the zoisite-rich layers are believed to be coeval with stage IVa. The kelyphite stages Va1 and Va2 may have been simultaneous; the difference in assemblage is probably caused by local variations in H_2O activity.

5.2. Textural/metamorphic development in the Ca–Al-poor compositions (dunite, harzburgite)

In Al-poor compositions, the earliest stage appears as a coarse-grained heterogranular rock consisting mainly of olivine and orthopyroxene with minor spinel. Based on the textural relationships, we suggest the following succession of metamorphic assemblages:

- Ib. Large Ol+Ca-rich Opx porphyroblasts+Cr-rich Spl.
- IIb. Medium- to fine-grained recrystallized Ol+Opx+Cr-rich Spl, with straining of stage Ib phases (Fig. 4c). Exsolution of clinopyroxene from original Ca-rich orthopyroxene (Fig. 5a).
- IIIb. Hydration and recrystallization with the development of a mosaic textured Ol±Tlc+Chl±Mgs with straight grain boundaries (Fig. 4d).

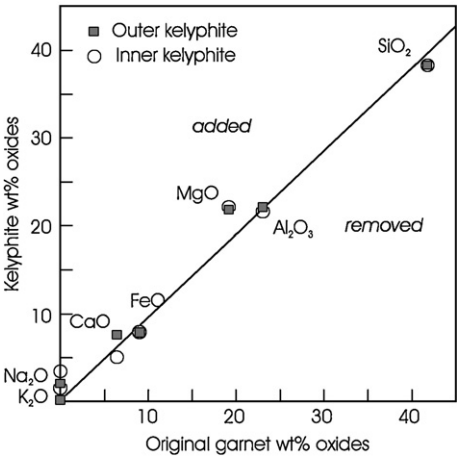

Fig. 7. Bulk compositions of outer hornblende–spinel and inner hornblende–chlorite kelyphite plotted against composition of garnet, showing metasomatic effects. Sample UM-2B.

- IVb. Poikiloblastic orthopyroxene (10–20 mm) overgrowth of stage IIIb assemblages (Fig. 4e).
- Vb. Ol+Chl+Amp (anthophyllite or tremolite)+Tlc+Mgs in a massive rock. A few rocks consist of poikiloblasts of anthophyllite with inclusions of olivine (Fig. 4f); orthopyroxene disappears from the stable assemblage.
- VIb. In the most altered rocks at the margins of the Langlitind body, Tlc+Mgs are common along with serpentine.

5.3. Metamorphic evolution

The earliest assemblage in dunitic/harzburgitic rocks from the Tromsø Nappe is probably represented by the coarse-grained porphyroclasts of olivine and orthopyroxene with exsolved clinopyroxene (stage Ib). The higher Ca-content of the pre-exsolution orthopyroxene indicates high temperatures.

The next stages would be Ia–IIIa, which implies progressive growth of garnet and consumption of spinel, which gradually becomes more Cr- and Fe-rich, until it apparently disappears. These stages thus show the transformation of the rocks from spinel to garnet peridotite through a *P–T* field where garnet and spinel coexisted with increasing pressure (e.g. Green and Ringwood, 1967; O'Neill, 1981; Asimov et al., 1995). The position of the spinel to garnet lherzolite in simple (e.g. CMAS) and more complex chemical systems (CFMAS) are well known (MacGregor, 1965; Green and Ringwood, 1967; Hales, 1969; O'Hara et al., 1971; O'Neill, 1981; Gasparik and Newton, 1984; Robinson and Wood, 1998; Klemme and O'Neill, 2000a,b). Minor

Table 8
Major and minor element compositions of ultramafic rocks from the Tromsø Nappe, recalculated to 100%

	UM-2A	UM-6	St-8
SiO_2	43.68	43.77	42.56
TiO_2	0.06	0.04	0.01
Al_2O_3	11.62	6.14	0.56
FeO (tot)	6.45	7.99	7.75
MnO	0.08	0.13	0.13
MgO	27.99	38.62	47.48
CaO	8.35	3.02	0.40
Na_2O	1.11	0.26	0.15
K_2O	0.13	0.03	0.00
Cr_2O_3	0.52	n.a.	n.a.
	100.00	100.00	100.00
Mg#	0.89	0.90	0.92

elements may, however, strongly influence this transition, and the effect of Cr has been addressed by several workers (MacGregor, 1970; Wood, 1978; O'Neill, 1981; Nickel, 1986; Webb and Wood, 1986; Doroshev et al., 1997; Brey et al., 1999; Girnis and Brey, 1999; Girnis et al., 2003; Klemme, 2004). The presence of Cr drastically increases the stability of spinel relative to garnet; the experimental results of Klemme (2004) show that the influence of Cr on the garnet–spinel transition is extraordinary, and is believed to exert a major control on phase relations in these systems. The recrystallized Ol+low-Ca Opx (stage IIb) in the dunite/harzburgite is probably isofacial with stage IIIa. The genuine maximum-*P* assemblage (IIIa) in the garnet-bearing peridotitic rock is not readily identifiable, but may have been the same as that found in the recrystallized and well foliated matrix. Thus we tentatively suggest that Grt+Cpx+pargasitic Hbl+Chl coexisted at maximum pressure conditions, and was later modified and recrystallized under non-static conditions (IVa). The garnet-orthopyroxenite (stage IVa′) and the zoisite-rich rocks were recrystallized coevally with this post maximum-*P* stage.

Kelyphitic rims of Opx±Cpx+Spl or Hbl+Spl around garnet (stages Va1 and Va2) appear to be formed under static conditions and decreasing *P*. In the dunitic/harzburgitic rocks hydration and recrystallization of the Ol+Opx assemblage to Ol±Tlc+Chl±Mgs (IIIb) indicate a drop in both *P* and *T*, with a succeeding near-isobaric increase in *T*, recorded by poikiloblastic orthopyroxene (IVb) overgrowing the previous assemblage. There does not seem to be any strong deformation of these assemblages, and they are suggested to be coeval with the kelyphite formation.

The next stages are characterized by the appearance of Ath+Tlc+Ol+Mgs and the disappearance of orthopyroxene at stage Vb in the dunitic/harzburgitic compositions, and the local development of an inner Na-rich kelyphite around garnet in the peridotitic compositions (VIa). The strong enrichment of Na in this kelyphite, mirrored by the highly sodic hornblende (ca. 4 wt.% Na_2O) and the nearby inclusions of albite in garnet, strongly suggest an influx of Na-rich fluids (Fig. 7).

The final stages recorded in the rocks involve further hydration with serpentinitization.

6. Geothermobarometry

The mineral chemistry for most minerals varies; apparently, equilibrium was not maintained during most of the metamorphic recrystallization. There is also strong evidence that much H_2O-rich fluid flushed through the rocks, enhancing disturbance of earlier equilibria. The use of common geothermometers based on the exchange of Fe^{2+} and Mg between phases is therefore highly risky as they would easily be reset as the rocks passed through different *P–T* conditions. The degree of thermal resetting is difficult to assess, but should be kept in mind when interpretations are made.

6.1. Pre-subduction stage

A temperature estimate for the early (pre-subduction) history based on bulk composition of orthopyroxene with exsolved clinopyroxene lamellae in the Stabben dunite gives 1337 °C at a *P* of 1.0 GPa, using the Ca-in-opx geothermometer of Brey and Köhler (1990). Bulk composition is obtained by scanning the cores of orthopyroxenes. This procedure will probably overestimate the density of lamellae and thus the calculated temperature. Nevertheless, the exsolution texture points to a pre-metamorphic high-*T* stage which may be of igneous, or possibly of mantle origin.

6.2. Early metamorphic stages (pre-maximum-P)

The early stages of the metamorphic evolution cannot be well constrained, but the coexistence of chlorite, hornblende, clinopyroxene and Cr-poor spinel as inclusions within garnet in the peridotitic compositions clearly points toward fairly low *T* at moderate *P*. Experiments on hydrous ultramafic systems comparable to (but not identical with) our rocks (Table 8) have been carried out by Niida and Green (1999) and Fumagalli and Poli (2005). Our sample UM-6 is fairly similar to the model MORB pyrolite (MPY) of Green et al. (1979), but differs from the MPY-40% olivine composition used

Table 9
P–T estimates for the stages 1–2 and 5 for the Holmevatn ultramafic body

Sample	Stage	P1 (GPa)	T1 (°C)	P2 (GPa)	T2 (°C)	P3 (GPa)	T2 (°C)
UM-2A spinel 1 (min Cr)	Pre-max-P 1a	1.39	677				
UM-2A spinel 2	Pre-max-P 1b	1.62	692				
UM-2A spinel 3	Pre-max-P 1c	1.78	702				
UM-2A spinel 4 (max Cr)	Pre-max-P 2	2.38	742				
UM-6		2.10	699				
02029-1	Post max-P 5			1.47	739	1.80	760
02031-1	Post max-P 5			1.63	757	1.90	774

Thermometers and barometers used are *T1*–Grt–Cpx Fe–Mg, Ravna (2000) *T2*–Grt–Opx Fe–Mg, Brey and Köhler (1990); *P1*–Grt–Cpx–Ol–Spl, this paper; *P2*–Al–in–Opx, Brey and Köhler, (1990); *P3*–Al–in–Opx, this paper.

by Niida and Green (1999). Our sample UM-2A is much higher in Al than any of the compositions used in these experiments. The experiments of Niida and Green (1999) were done under H_2O undersaturated conditions at 925 to 1100 °C and 0.4 to 3.2 GPa, which apparently are quite different from the conditions experienced by our rocks. Fumagalli and Poli (2005) performed their experiments at fluid saturated conditions at 688 to 800 °C and 2.0 to 6.5 GPa, conditions that are relevant for our rocks. However, they used Cr-free compositions, which certainly affects the stability relations of spinel, as this phase is absent in their runs. Thus, taking the experimental conditions and bulk compositions used in these two sets of experiments, none of them will apply to the present rocks.

Conventional geothermobarometry on the present rocks appears to be risky due to widespread indications of chemical disequilibrium. Fe–Mg exchange thermometers are known to be readily disturbed during a metamorphic cycle (Ravna and Paquin, 2003 and references therein). This is well documented here by the highly variable Mg# of olivine from the same thin section, and even the same grain. The use of the garnet–olivine Fe–Mg thermometer (Brey and Köhler, 1990; O'Neill and Wood, 1979; O'Neill, 1980) has thus been avoided in this paper. As clinopyroxene, orthopyroxene and garnet show fairly constant and homogeneous Mg# within each sample, these phases are used for thermometry here (Bertrand and Mercier, 1985; Brey and Köhler, 1990; Ravna, 2000).

Pressure estimates for the orthopyroxene-absent Ca–Al rich assemblages are not readily obtained, but the reaction

$$6\,CaMgSi_2O_6 + 3MgAl_2O_4 = Mg_3Al_2Si_3O_{12} + 2Ca_3Al_2Si_3O_{12} + 3Mg_2SiO_4$$

$$6\,\text{diopside} + 3\,\text{spinel} = \text{pyrope} + 2\,\text{grossular} + 3\,\text{forsterite}$$

may serve as a potential geobarometer (see Appendix).

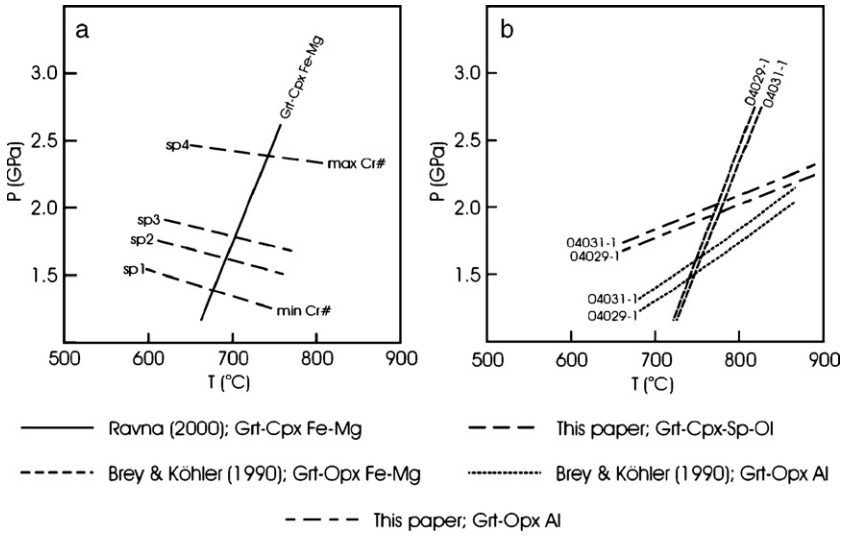

Fig. 8. *P–T* calculations based on coexisting (a) garnet–clinopyroxene–olivine–spinel (sample UM-2A) and (b) garnet–orthopyroxene (samples 04028-1 and 04031-1).

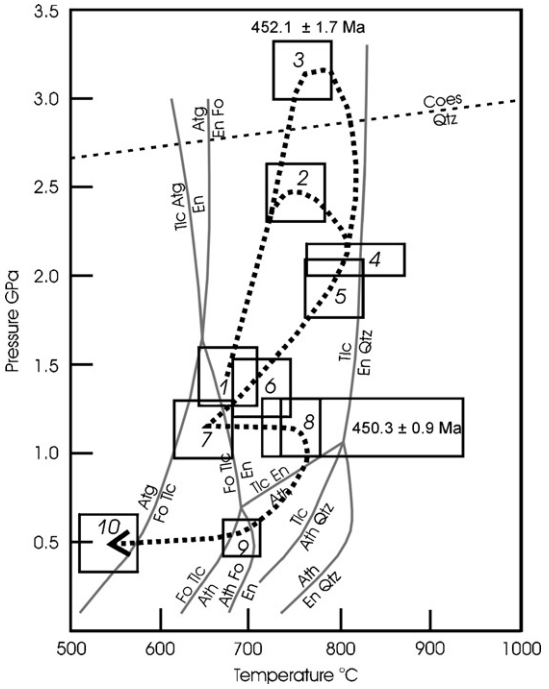

Fig. 9. *P–T* grid for MFSH (Mg#=90; dunite/harzburgite) calculated from THERMOCALC, with approximate positions for the different metamorphic stages based on the observed succession of mineral parageneses and *P–T* estimates. NB! The *P–T* boxes for each stage do not represent real uncertainties.

For the garnet–orthopyroxene assemblage in the garnet-orthopyroxenite, the Al-in-orthopyroxene coexisting with garnet geobarometer (Brey and Köhler, 1990) is used, along with a linearized expression for the reaction (see Appendix)

$$Mg_3Al_2Si_3O_{12} = Mg_2Si_2O_6 + MgAlAlSiO_6$$

$$\text{pyrope} = \text{enstatite} + \text{mg} - \text{tschermakite}$$

For the Ca-Al rich assemblages involving successive inclusions of spinel and clinopyroxene in garnet coexisting with olivine in sample UM-2A a combination of the garnet–clinopyroxene Fe–Mg thermometer (Ravna, 2000) and the garnet–clinopyroxene–spinel–olivine barometer (this paper) will record the early *P–T* conditions using. A theoretical value for olivine coexisting with garnet at 750 °C and 1.5 to 2.0 GPa will be Fo_{92} (Brey and Köhler, 1990), somewhat more magnesian than analyzed matrix olivine ($Fo_{84–87}$). As garnet, olivine and clinopyroxene together with hornblende and chlorite were major phases compared with spinel during the stage of garnet growth, we expect that the composition of spinel would readily change, whereas the other minerals would show only minor changes. Thus a combination of garnet with the fictive olivine composition given above and clinopyroxene+spinel inclusions in garnet will monitor the relative changes in *P* through stages Ia to IIa. The results (Table 9; Fig. 8a) are promising, showing an increase in *P* from inclusion suite 1 (minimum Cr# of spinel) of 1.40 GPa at 675 °C, through inclusion suite 2 and 3 (1.60 GPa/690 °C and 1.80 GPa/700 °C, respectively) to inclusion suite 4 (maximum Cr# in spinel; 2.40 GPa/740 °C). These *P* estimates should, however, not be taken as accurate as error limits appear to be rather large (sd*P*=0.44 GPa according to THERMOCALC). If the maximum Mg# olivine in Table 6 is used instead of the estimated Fo_{90}, calculated *P* will be 0.12 GPa lower. Nevertheless the *P* estimates are very reasonable, and more importantly, the relative changes in *P* are unambiguous.

6.3. Maximum-P conditions

As spinel is absent from the matrix assemblage, maximum *P* may have been higher than calculated for spinel inclusion suite 4. In dunite/harzburgite, the assemblage Ol+Opx would be stable at *T*>700 °C. Recent results (Ravna and Roux, in press) indicate pressures as high as 3.36 GPa at 735 °C for nearby eclogites based on the assemblage Grt–Cpx–Phe, conditions that most probably also are valid for the present ultramafic rocks.

6.4. Post maximum-P and pre-kelyphite decompression

The *P–T* conditions for post peak-*P* and pre-kelyphite stage can be obtained from the mineral assemblage Grt+Opx from the garnet-orthopyroxenite samples 04029-1 and +4031-1. A combination of the garnet–orthopyroxene Fe–Mg thermometer and the Al-in-orthopyroxene geobarometers (Brey and Köhler, 1990; this paper) give 1.5–1.6 GPa at 750 °C and c. 2.0 GPa at 775 °C, respectively (Table 9; Fig. 8b). An "average *PT*" calculation on the assemblage Grt+Hbl+Zo+Chl observed in the zoisite-rich rock (e.g. sample 04029-1A) gives 740±32 °C, 1.75±0.26 GPa using THERMOCALC (Powell and Holland, 1988; Holland and Powell, 1998). It is thus suggested that the post maximum-*P* and pre-kelyphite foliation was formed at 750±50 °C and 1.75±0.25 GPa.

6.5. Kelyphite formation

The formation of kelyphitic rims of Opx±Cpx+Spl (virtually Cr-free) and Hbl+Spl around garnet poikiloblasts is a result of further decompression at static conditions. According to the experimental work of

Klemme and O'Neill (2000a,b), the garnet to spinel lherzolite transition in the Cr-free CMAS system is located at around 1.5 GPa at 700–800 °C. The addition of Fe to this system will lower this transition (O'Neill, 1981). An attempt to estimate the temperature for this event from Cpx+Opx associated with kelyphite in sample 04028 (Fig. 5b) yields 700–725 °C at P range 1.0–1.5 GPa, using the two-pyroxene thermometers of Bertrand and Mercier (1985) and Brey and Köhler (1990).

6.6. Breakdown and regrowth of orthopyroxene in dunite/harzburgite

In the dunitic compositions the assemblage orthopyroxene breaks down to Ol+Tlc. This assemblage has a narrow T stability field of 610–690 °C at P=1.0–1.5 GPa, while the succeeding orthopyroxene overgrowth is stable at T>700 °C (Fig. 9). The lower P limit for the assemblage orthopyroxene (host)+talc (inclusion) defined by the reaction

$$\text{talc} + \text{enstatite} = \text{anthophyllite}$$

is between 1.1 GPa at 800 °C and 0.7 GPa at 690 °C, and the upper temperature stability of talc, limited by the reaction

$$\text{talc} = \text{enstatite} + \text{quartz} + H_2O$$

is 800 °C (Fig. 9). The large anthophyllite poikiloblasts with inclusions of olivine (Fig. 4f) may represent pseudomorphs of the poikiloblastic orthopyroxene, formed at P below 1.0 GPa at T around 700 °C. The final observed stages involving growth of antigorite and other serpentine polymorphs in all ultramafic rock types happened at T<550 °C.

A summary of the metamorphic evolution of the Tromsø Nappe ultramafic rocks is shown in Fig. 9.

7. Discussion

The peridotitic to dunitic rocks from the Tromsø Nappe show a complex metamorphic history, giving well documented evidence of a prograde subduction-related evolution, with a pressure increase of at least 1 GPa during garnet growth along a relatively cool P/T gradient. The rough P–T estimates presented in this paper differ from those presented by Krogh et al. (1990) on eclogites, but newer methods (Ravna and Terry, 2004) and additional unpublished data (Ravna and Roux, in press) put the maximum pressure for the eclogites at 3.36 GPa at c. 735 °C. The P–T evolution of the present rocks based on textural observations and thermobarometry indicate a moderate increase in T during the initial phases of uplift (Fig. 9), succeeded by cooling at further uplift, and then by an event of approximately isobaric heating before final cooling and decompression. This is in line with the observed appearance of two separate stages of decompression partial melting observed in eclogites from the area (Stevenson, 2005), the oldest involving peritectic garnet occurring at 2.0–2.2 GPa, 762–844 °C and the youngest involving peritectic hornblende at 1.0–1.3 GPa, 743–950 °C. The uplift of the deeply subducted terrane has been very rapid, as shown by the geochronological work of Corfu et al. (2003). Maximum P conditions were reached at 452.1±1.7 Ma, whereas the hornblende-bearing leucosomes are dated to 450.3±0.9 Ma. The last heating event with consequent partial melting may be related to tectonic juxtaposition of the Tromsø Nappe and the still hot underlying Skattøra Migmatite Complex of the Nakkedal Nappe, where extensive partial melting at around 1.0 GPa and 900 °C took place at 456±4 Ma (Selbekk et al., 2000; Selbekk and Skjerlie, 2002).

The protoliths have been variably hydrated prior to the subduction; thus assemblages of pre-subduction (igneous or mantle related) stages have been preserved in the least hydrated rocks. Other protoliths have been extensively hydrated, giving rise to an early assemblage of pargasitic Hbl+Chl, with minor Cr-poor spinel and clinopyroxene. The ultramafic rocks are closely associated with eclogites and various metasediments (Krogh et al., 1990), and have shared the same complex subduction-related metamorphic history. At the Holmevatn locality (Fig. 1) the ultramafic rocks are exposed only a few meters from a large eclogite body, but the boundary is not exposed. We suggest that the ultramafic rocks, at least at this locality, represent the cumulate sequence of a larger layered mafic complex, although we so far have no geochemical evidence for such an interpretation.

8. Summary of P–T evolution

A summary based on the observed textural observations and geothermometric estimates is given in Fig. 9.

1. Stage 1 is represented by Cpx+Hbl+Chl+low-Cr Spl included in garnet, with olivine as an additional phase. Estimated P–T conditions are 1.4 GPa/675 °C.
2. The mineral assemblage Grt+Cpx+Hbl+Chl+Spl (Cr-rich) is apparently stable up to c. 2.4 GPa and 740 °C, where spinel seems to disappear.

3. Maximum *P–T* conditions for nearby eclogites give UHP conditions of up to 3.36 GPa at 735 °C (Ravna and Roux, in press).
4. Post maximum-*P* conditions pass through conditions where partial melting of eclogites involving peritectic garnet is formed at 2.0–2.2 GPa and 760–845 °C (Stevenson, 2005).
5. Main foliation and recrystallization occurred at c. 2.0 GPa and 740–780 °C.
6. Formation of kelyphites around garnet occurred at $P<1.5$ GPa and 700–725 °C.
7. Orthopyroxene breakdown to Ol+Tlc occurred at $P<1.5$ GPa and $T<650$–700 °C.
8. Increasing T (to >700 °C) at approximately isobaric conditions causes overgrowth of poikiloblastic orthopyroxene on Ol+Tlc and partial melting of eclogite involving peritectic hornblende (Stevenson, 2005).
9. Breakdown of orthopyroxene to anthophyllite +olivine occurred by cooling and unloading at $P<1.0$ GPa and $T\sim700$ °C.
10. Further cooling and hydration produces serpentine.

Acknowledgements

We wish to acknowledge the thorough and constructive reviews of J.G. Liou and E. Essene, which added important improvements to this work. We will also thank G. Corner for correcting the English language, and T.I. Eilertsen for keeping the analytical equipment in top condition.

Appendix A. Appendix

For geobarometric purposes we have used the program THERMOCALC (Powell and Holland, 1988) and the thermodynamic database of Holland and Powell (1998) to obtain linearized expressions of two important reactions involving common phases in garnet-bearing ultramafic rocks. The reaction

$$6CaMgSi_2O_6 + 3MgAl_2O_4 = 2Ca_3Al_2Si_3O_{12} + Mg_3Al_2Si_3O_{12} + 3Mg_2SiO_4$$

$$6\,\text{diopside} + 3\,\text{spinel} = 2\,\text{grossular} + 1\,\text{pyrope} + 3\,\text{forsterite}$$

is one of the principal reactions in the transition from spinel to garnet peridotite, and is an equivalent to the commonly used and corresponding reaction involving orthopyroxene. At 750 °C and 2.0 GPa, this reaction has a rather flat lying slope in the *P–T* diagram through the linearized equation

$$P(\text{GPa}) = \left[0.550 + 0.003110*T + 0.000373 *T*\ln\frac{a_{fo}^3 * a_{pyr} * a_{grs}^2}{a_{di}^6 * a_{sp}^3}\right]$$

This reaction is a potential geobarometer, and has been used to estimate pressures for the orthopyroxene-free assemblages in the present paper. Estimated uncertainty sd$P$ is 0.44 GPa according to THERMOCALC. The reaction

$$Mg_3Al_2Si_3O_{12} = Mg_2Si_2O_6 + MgAlAlSiO_6$$

$$\text{Pyr} = \text{En} + \text{Mgts}$$

has an intermediate slope in the *P–T* diagram and has been widely used as a valuable geobarometer (Harley, 1984; Harley and Green, 1982; Brey and Köhler, 1990). In this paper we have obtained a linearized expression at 750 °C and 2.0 GPa of this geobarometer given as

$$P(\text{GPa}) = \left[-1.035 + 0.0000759*T + 0.00105 *T*\ln\frac{a_{pyr}}{a_{mgts} * a_{en}}\right]$$

Estimated uncertainty sd$P$ is 0.38 GPa according to THERMOCALC.

Activities for pyroxenes, olivine and spinel are calculated from the program *AX* (Holland; http://www.esc.cam.ac.uk/astaff/holland/ax.html), and for garnet the activity model of Ganguly et al. (1996) is used.

References

Asimov, P.D., Hirschmann, M.M., Ghiorso, M.S., O'Hara, M.J., Stolper, E.M., 1995. The effect of pressure induced solid–solid phase transitions on decompression melting of the mantle. Geochim. Cosmochim. Acta 59, 4489–4506.

Bertrand, P., Mercier, J.-C.C., 1985. The mutual solubility of coexisting ortho- and clinopyroxene: toward an absolute geothermometer for the natural system? Earth Planet. Sci. Lett. 76, 109–122.

Brey, G.P., Doroshev, A.M., Girnis, A.V., Turkin, A.I., 1999. Garnet–spinel–olivine–orthopyroxene equilibria in the FeO–MgO–Al_2O_3–SiO_2–Cr_2O_3 system: I. Composition and molar volumes of minerals. Eur. J. Mineral. 11, 599–717.

Brey, G.P., Köhler, T., 1990. Geothermobarometry in four-phase lherzolites: II. New thermobarometers and practical assessment of existing thermobarometers. J. Petrol. 31, 1353–1378.

Broks, T.M., 1985. Berggrunnsgeologiske undersøkelser innen Tromsø dekkekompleks i området Tromsdalen–Ramfjord–Breivikeidet, Troms. Unpubl. Cand. Scient. Thesis, University of Tromsø (in Norwegian).

Brueckner, H.K., Medaris, L.G., 2000. A general model for the intrusion and evolution of 'mantle' garnet peridotites in high-pressure and ultra-high-pressure metamorphic terranes. J. Metamorph. Geol. 18, 123–133.

Bucher-Nurminen, K., 1991. Mantle fragments in the Scandinavian Caledonides. Tectonophysics 190, 173–192.

Carswell, D.A., Cuthbert, S.J., 2003. Ultrahigh pressure metamorphism in the western Gneiss Region of Norway. In: Carswell, D.A., Compagnoni, R. (Eds.), Ultrahigh Pressure Metamorphism. EMU Notes in Mineralogy, vol. 5, pp. 51–53. Ch. 3.

Corfu, F., Ravna, E.J.K., Kullerud, K., 2003. A Late Ordovician U–Pb age for the Tromsø Nappe eclogites, uppermost allochthon of the Scandinavian Caledonides. Contrib. Mineral. Petrol. 145, 502–513.

Dallmeyer, R.D., Andresen, A., 1992. Polyphase tectonothermal evolution of exotic Caledonian nappes in Troms, Norway: evidence from $^{40}Ar/^{39}Ars$ mineral ages. Lithos 29, 19–42.

Doroshev, A.M., Brey, G.P., Girnis, A.V., Turkin, A.I., Kogarko, L.N., 1997. Pyrope–knorringite garnets in the Earth's mantle: experiments in the $MgO–Al_2O_3–SiO_2–Cr_2O_3$ system. Russ. Geol. Geophys 38, 559–586.

Ellingsen, E., 1997. Metamorfose av ultramafiske bergarter i Tromsdalstindsekvensen, Tromsø dekkekompleks. Unpublished Cand. Scient. thesis, University of Tromsø (in Norwegian).

Enami, M., Zhang, Q., 1988. Magnesian staurolite in garnet–corundum rocks and eclogite from the Donghai District, Jiangsu Province, east China. Am. Mineral. 73, 48–56.

Ernst, W.G., 1978. Petrochemical study of lherzolitic rocks from the western Alps. J. Petrol. 19, 341–392.

Evans, B.W., Trommsdorff, V., 1978. Petrogenesis of garnet lherzolite, Cima di Gagnone, Lepontine Alps. Earth Planet. Sci. Lett. 40, 333–348.

Fumagalli, P., Poli, S., 2005. Experimentally determined phase relations in hydrous peridotites to 6.5 GPa and their consequences on the dynamics of subduction zones. J. Petrol. 46, 555–578.

Ganguly, J., Cheng, W., Tirone, M., 1996. Thermodynamics of aluminosilicate garnet solid solution: new experimental data, an optimized model, and thermometry applications. Contrib. Mineral. Petrol. 126, 137–151.

Gasparik, T., Newton, R.C., 1984. The reversed alumina contents of orthopyroxene in equilibrium with spinel and forsterite in the system $MgO–Al_2O_3–SiO_2$. Contrib. Mineral. Petrol. 85, 186–196.

Girnis, A.V., Brey, G.P., 1999. Garnet–spinel–olivine–orthopyroxene equilibria in the $FeO–MgO–Al_2O_3–SiO_2–Cr_2O_3$ system: II. Thermodynamic analysis. Eur. J. Mineral. 11, 619–636.

Girnis, A.V., Brey, G.P., Doroshev, A.M., Turkin, A.I., Simon, N., 2003. The system $MgO–Al_2O_3–SiO_2–Cr_2O_3$ revisited: reanalysis of Doroshev et al.'s (1977) experiments and new experiments. Eur. J. Mineral. 15, 953–964.

Green, D.H., Ringwood, A.E., 1967. The stability field of aluminous pyroxene peridotite and garnet peridotite and their relevance in upper mantle structure. Earth Planet. Sci. Lett. 3, 151–160.

Green, D.H., Hibberson, W.O., Jaques, A.L., 1979. Petrogenesis of mid ocean ridge basalt. In: McElhinney, M.W. (Ed.), The Earth: its origin structure and evolution. Academic Press, London, pp. 265–299.

Hales, A.L., 1969. A seismic discontinuity in the lithosphere. Earth Planet Sci. Lett. 7, 44–46.

Harley, S.L., 1984. The solubility of alumina in orthopyroxene coexisting with garnet in $FeO–MgO–Al_2O_3–SiO_2$ and $CaO–FeO–MgO–Al_2O_3–SiO_2$. J. Petrol. 25, 665–696.

Harley, S.L., Green, D.H., 1982. Garnet-orthopyroxene barometry for granulites and peridotites. Nature 300, 697–701.

Holland, T.J.B., Powell, R., 1998. An internally consistent thermodynamic data set for phases of petrological interest. J. Metamorph. Geol. 16, 309–343.

Ibarguchi, J.I.G., Mendia, M., Girardeau, J., 1991. Mg- and Cr-rich staurolite and Cr-rich kyanite in high-pressure ultramafic rocks (Cabo Ortegal, northwestern Spain). Am. Mineral. 76, 501–511.

Kadarusman, A., Parkinson, C.D., 2000. Petrology and *P–T* evolution of garnet peridotites from central Sulawesi, Indonesia. J. Metamorph. Geol. 18, 193–209.

Kalt, A., Altherr, R., 1996. Metamorphic evolution of garnet–spinel peridotites from the Variscan Schwarzwald (Germany). Geol. Rundsch. 85, 211–224.

Klemme, S., 2004. The influence of Cr on the garnet–spinel transition in the Earth's mantle: experiments in the system $MgO–Cr_2O_3–SiO_2$ and thermodynamic modeling. Lithos 77, 639–646.

Klemme, S., O'Neill, H.S.C., 2000a. The effect of Cr on the solubility of Al in orthopyroxene: experiments and thermodynamic modeling. Contrib. Mineral. Petrol. 140, 84–98.

Klemme, S., O'Neill, H.S.C., 2000b. The near-solidus transition from garnet lherzolite to spinel lherzolite. Mineral. Petrol. 138, 237–248.

Kretz, R., 1983. Symbols for rock-forming minerals. Am. Mineral. 68, 277–279.

Krogh, E.J., Carswell, D.A., 1995. HP and UHP eclogites and garnet peridotites in the Scandinavian Caledonides. In: Coleman, R.G., Wang, X. (Eds.), Ultrahigh Pressure Metamorphism. Cambridge University Press, Cambridge, pp. 244–297.

Krogh, E.J., Andresen, A., Bryhni, I., Broks, T.M., Kristensen, S.E., 1990. Eclogites and polyphase *P–T* cycling in the Caledonian uppermost allochthon in Troms, northern Norway. J. Metamorph. Geol. 8, 289–309.

Liou, J.G., Zhang, R.Y., 1998. Petrogenesis of an ultrahigh-pressure garnet-bearing ultramafic body from Maowu, Dabie Mountains, east-central China. Isl. Arc 7, 115–134.

MacGregor, I.D., 1965. Stability fields of spinel and garnet peridotites in the synthetic system $MgO–CaO–Al_2O_3–SiO_2$. Year-b. Carnegie Inst. Washington 64, 126–134.

MacGregor, I.D., 1970. The effect of CaO, Cr_2O_3, Fe_2O_3 and Al_2O_3 on the stability of spinel and garnet peridotites. Phys. Earth Planet. Inter. 3, 372–377.

Medaris, L.G., 2000. Garnet peridotites in Eurasian high-pressure and ultrahigh-pressure terranes: a discovery of origins and thermal histories. In: Ernst, W.G., Liou, J.G. (Eds.), UHP Metamorphism and Geodynamics in Collision Type Orogenic Belts. Boulder, CO: Geol. Soc. Am. , pp. 57–73.

Medaris, L.G., Carswell, D.A., 1990. Petrogenesis of Mg–Cr garnet peridotites in European metamorphic belts. In: Carswell, D.A. (Ed.), Eclogite Facies Rocks. Blackie, Glasgow London, pp. 260–290.

Medaris, L.G., Wang, H.F., Misar, Z., Jelinek, E., 1990. Thermobarometry, diffusion and cooling rates of crustal garnet peridotites-2 examples from the Moldanubian Zone of the Bohemian Massif. Lithos 25, 189–202.

Morten, L., Trommsdorff, V., 2003. Metamorphism and textures of dry and hydrous garnet peridotites. EMU Notes Mineral. 5, 443–466 Ch 14.

Nickel, K.G., 1986. Phase equilibria in the system SiO_2–MgO–Al_2O_3–CaO–Cr_2O_3 (SMACCR) and their bearing on spinel/garnet lherzolite relationships. N. Jahrb. Mineral. Abh. 155, 259–287.

Nicollet, C., 1986. Sapphirine and Mg-rich, Cr-rich Staurolite in Corundum-bearing amphibolite and anorthosite from Vohibory, Madagascar. Bull. Minéral. 109, 599–612.

Niida, K., Green, D.H., 1999. Stability and chemical composition of pargasitic amphibole in MORB pyrolite under upper mantle conditions. Contrib. Mineral. Petrol. 135, 18–40.

Nimis, P., Morten, L., 2000. *P–T* evolution of 'crustal' garnet peridotites and included pyroxenites from Nonsberg area (upper Austroalpine), NE Italy: from the wedge to the slab. J. Geodyn. 30, 93–115.

Obata, M., Morten, L., 1987. Transformation of spinel lherzolite to garnet lherzolite in ultramafic lenses of the Austridic Crystalline Complex, northern Italy. J. Petrol. 28, 599–623.

O'Hara, M.J., Richardson, S.W., Wilson, G., 1971. Garnet peridotite stability and occurrence in crust and mantle. Contrib. Mineral. Petrol. 32, 48–68.

O'Neill, H.S.C., 1980. An experimental study of Fe-Mg partitioning between garnet and olivine and its calibration as a geothermometer: Corrections. Contrib. Mineral. Petrol. 72, 337.

O'Neill, H.S.C., 1981. The transition between spinel lherzolite and garnet lherzolite, and its use as a geobarometer. Contrib. Mineral. Petrol. 77, 185–194.

O'Neill, H.S.C., Wood, B.J., 1979. Experimental study of Fe-Mg partitioning between garnet and olivine and its calibration as a geothermometer. Contrib. Mineral. Petrol. 70, 59–70.

Paquin, J., Altherr, R., 2001. New constraints on the *P–T* evolution of the Alpe Arami garnet peridotite body (central Alps, Switzerland). J. Petrol. 42, 1119–1140.

Powell, R., Holland, T.J.B., 1988. An internally consistent thermodynamic dataset with uncertainties and correlations. 3. Applications to geobarometry, worked examples and a computer program. J. Metamorph. Geol. 6, 173–204.

Ravna, E.J.K., 2000. The garnet–clinopyroxene geothermometer — an updated calibration. J. Metamorph. Geol. 18, 211–219.

Ravna, E.J.K., Paquin, J., 2003. Thermobarometric methodologies applicable to eclogites and garnet ultrabasites. In: Carswell, D.A., Compagnoni, R. (Eds.), Ultrahigh Pressure Metamorphism. EMU Notes in Mineralogy, vol. 5, pp. 229–259. Ch. 8.

Ravna, E.J.K., Terry, M.P., 2004. Geothermobarometry of UHP and HP eclogites and schists — an evaluation of equilibria among garnet–clinopyroxene–kyanite–phengite–coesite/quartz. J. Metamorph. Geol. 22, 579–592.

Ravna, E.J.K., Roux, M.R.M., in press. Metamorphic evolution of the Tønsvika eclogite, Tromsø Nappe - evidence for a new UHPM province in the Scandinavian Caledonides. Int. Geol. Rev.

Robinson, J.A., Wood, B.J., 1998. The depth of the spinel to garnet transition at the peridotite solidus. Earth Planet. Sci. Lett. 164, 277–284.

Selbekk, R.S., Skjerlie, K.P., 2002. Petrogenesis of the anorthosite dyke swarm of Tromsø, North Norway: experimental evidence for hydrous anatexis of an alkaline mafic complex. J. Petrol. 43, 943–962.

Selbekk, R.S., Skjerlie, K.P., Pedersen, R.B., 2000. Generation of anorthositic magma by H_2O-fluxed anatexis of silica-undersaturated gabbro: an example from the north Norwegian Caledonides. Geol. Mag. 137, 609–621.

Stevenson, J.A. 2005, High pressure partial melting of eclogite and garnet amphibolite rocks during decompression and heating, Tromso Nappe, Norway. EOS, Transactions AGU, 85 (47), Abstract T23C-03.

Ward, C.M., 1984. Magnesium staurolite and green chromian staurolite from Fiordland, New Zealand. Am. Mineral. 69, 531–540.

Webb, S.A., Wood, B.J., 1986. Spinel–pyroxene–garnet relationships and their dependence on Cr/Al ratio. Contrib. Mineral. Petrol. 92, 471–480.

Wood, B.J., 1978. The influence of Cr_2O_3 on the relationships between spinel- and garnet peridotites. In: MacKenzie, W.S. (Ed.), Progress in Experimental Petrology. NERC, Manchester, pp. 78–80.

Zhang, R.Y., Liou, J.G., Bolin, C., 1994. Petrogenesis of garnet-bearing ultramafic rocks and associated eclogites in the Su-Lu ultrahigh-*P* metamorphic terrane, eastern China. J. Metamorph. Geol. 12, 169–186.